Human and murine fibroblast single cell transcriptomics reveals fibroblast clusters are differentially affected by ageing, and serum cholesterol

Human and murine fibroblast single cell transcriptomics reveals fibroblast clusters are differentially affected by ageing, and serum cholesterol

Fibroblast clusters in health and disease

van Kuijk K[1,2], McCracken IR[3], Tillie RJHA[1], Asselberghs SEJ[1,4], Kheder DA[1], Muitjens S[1], Jin H[1], Taylor RS[3], Wichers Schreur R[1], Kuppe C[2,5], Dobie R[6], Ramachandran P[6], Gijbels MJ[1,7,8], Temmerman L[1], Kirkwoord PM[6], Luyten J[1,4], Li Y[9,10], Noels H[11], Goossens P[1], Wilson-Kanamori JR[5], Schurgers LJ[1,2], Shen YH [9,10], Mees BME[1,4], Biessen EAL[1,11], Henderson NC[5,12], Kramann R[2,4], Baker AH[1,3], Sluimer JC[1,3]

[1] Cardiovascular Research Institute Maastricht (CARIM), Maastricht University Medical Center, Maastricht, Netherlands; [2] Institute of Experimental Medicine and Systems Biology, Faculty of Medicine, RWTH Aachen University, Aachen, Germany; [3] BHF Centre for Cardiovascular Sciences (CVS), University of Edinburgh, Edinburgh, UK; [4] Department of Vascular Surgery, Maastricht University Medical Center, Maastricht, Netherlands; [6] Division of Nephrology and Clinical Immunology, Faculty of Medicine, RWTH Aachen University, Aachen, Germany; [6] Centre for Inflammation Research, University of Edinburgh, Edinburgh, UK; [7] Department of Medical Biochemistry, Experimental Vascular Biology, Amsterdam UMC, Amsterdam, The Netherlands; [8]GROW, School for Oncology and Development Biology, Maastricht University, Maastricht, The Netherlands; [9]Division of Cardiothoracic Surgery, Baylor College of Medicine, Houston, TX; [10] Department of Cardiovascular Surgery, Texas Heart Institute, Houston; [11] Institute for Molecular Cardiovascular Research, RWTH Aachen University, Aachen, Germany; [12] MRC Human Genetics Unit, Institute of Genetics and Cancer, University of Edinburgh, Edinburgh, UK

Corresponding author: Judith Sluimer, Pathology department, MUMC, P. Debyelaan 25 6229HX Maastricht. Tel: +31(0)433877675, Fax +31(0)433876613,
Email: judith.sluimer@maastrichtuniversity.nl

Category: Original article
Word count: 9501

Abstract

Aims: Specific fibroblast markers and in-depth heterogeneity analysis are currently lacking, hindering functional studies in cardiovascular diseases (CVD). Here, we established cell-type markers and heterogeneity in murine and human arteries and studied the adventitial fibroblast response to CVD and its risk factors hypercholesterolemia and aging.

Methods & Results: Murine aorta scRNA-seq analysis of adventitial mesenchymal cells identified fibroblast-specific markers. Immunohistochemistry and flow cytometry validated platelet-derived growth factor receptor alpha (PDGFRA) and dipeptidase 1 (DPEP1*)* across human and murine aorta, carotid, and femoral arteries, while traditional markers such as cluster of differentiation (CD)90 and vimentin also marked transgelin+ vascular smooth muscle cells. Next, pseudotime analysis showed multiple fibroblast clusters differentiating along trajectories. Three trajectories, marked by CD55 (*Cd55*+), Cxcl chemokine 14 *(Cxcl14*+) and lysyl oxidase (*Lox*+), were reproduced in an independent RNAseq dataset. Gene ontology analysis showed divergent functional profiles of the three trajectories, related to vascular development, antigen presentation and/or collagen fibril organization, respectively. Trajectory-specific genes included significantly more genes with known genome-wide associations (GWAS) to CVD than expected by chance, implying a role in CVD. Indeed, differential regulation of fibroblast clusters by CVD risk factors was shown in adventitia of aged C57BL/6J mice, and mildly hypercholesterolemic LDLR-KO mice on chow by flow cytometry. The expansion of collagen-related CXCL14+ and LOX+ fibroblasts in aged and hypercholesterolemic aortic adventitia respectively, coincided with increased adventitial collagen. Immunohistochemistry, bulk, and single-cell transcriptomics of human carotid and aorta specimens emphasized translational value as CD55+, CXCL14+ and LOX+ fibroblasts were observed in healthy and atherosclerotic specimens. Also, trajectory-specific gene sets differentially correlated to human atherosclerotic plaque traits.

Conclusion: We provide two adventitial fibroblast-specific markers, PDGFRA and DPEP1, and demonstrate fibroblast heterogeneity in health and cardiovascular disease in humans and mice. Biological relevance is evident from regulation of fibroblast clusters by age and hypercholesterolemia *in vivo*, associations with human atherosclerotic plaque traits, and enrichment of genes with a GWAS for CVD.

Key words: Adventitia, Fibroblasts, Heterogeneity, Atherosclerosis, Single-cell RNA-Seq

Translational prospective

The current study sheds light on the transcriptional heterogeneity of arterial fibroblasts and the influence of pathologic environments, such as lipid levels or aging, on fibroblast differentiation through transcriptional trajectories. In addition, the presence of fibroblast clusters in human specimens and their enrichment of genes associated with CVD, highlight their potential role in disease development and progression. Novel therapeutic strategies could be shifting the focus to cell-specific targeting. By influencing fibroblast differentiation, their functional properties could be altered as well, e.g. adapting pro-fibrotic potential. This could be of great importance in regulating the effect of fibroblasts on CVD.

Introduction

Cellular heterogeneity and plasticity are two fundamental concepts that are beginning to define both the healthy and diseased vasculature[1]. This challenges the traditional approach to understanding previously distinct cellular compartments in the blood vessel wall, and the identities of cells that infiltrate the vessel wall in disease[2]. One cell type in particular, known for its high plasticity and heterogeneity in numerous organs is the fibroblast[3-5]. Fibroblasts mostly reside in the adventitial layer of the arterial wall, accompanied by other mesenchymal cells (e.g. pericytes and smooth muscle cells (SMCs)), immune cells and connective tissue[6]. Mainly fibroblasts express the stem cell marker Sca-1/Ly6a, underpinning the potential of these cells to be reprogrammed into a diverse cell repertoire, supporting extensive plasticity[7, 8]. Their functional role in fibrosis, inflammation, and angiogenesis in other organs[9, 10] makes these cells an attractive candidate for therapeutic intervention in arterial pathologies, such as atherosclerosis and vascular ageing. However, presumably also due to this plasticity, markers specifically distinguishing fibroblasts at the mRNA and protein level from other vascular cells have been very difficult to define. For example, traditional markers such as collagen 1 alpha 1 (*Col1α1*), collagen 1 alpha 2 (*Col1α2*), fibroblast activation protein (*Fap*) and fibroblast specific protein-1 (*Fsp-1*) lack the ability to distinguish between fibroblasts and other vascular cell types[11]. In addition, other vascular mesenchymal cells exhibit phenotypes resembling that of fibroblasts upon vascular challenges[12, 13]. Nevertheless, these markers have been used to detect fibroblast-like cells, originating from SMCs, or endothelial cells in atherosclerosis [13-15]. Thus, there is a need to resolve their fibroblast specificity to discern the impact or limitations of these studies. In addition, the role and regulation of potential fibroblast heterogeneity in vascular health and disease is not explored in sufficient detail but understanding disease-stimulating or -preventing phenotypes may impact therapeutic approaches.

Single-cell RNA sequencing (scRNA-seq) and concomitant extensive validation could resolve the ambiguity of fibroblast identity markers and potential heterogeneity. Indeed, scRNA-seq has been key in identifying pan fibroblast-specific markers across the microvasculature in several major organs compared to mural cells (consisting of pericytes and SMCs)[16]. Yet, it remains to be defined which markers are specific for arterial adventitial fibroblasts compared to other arterial cells. Previous scRNA-seq analyses of healthy murine vasculature have described transcriptomics of all arterial wall cell types, including fibroblasts, in a so called atlas approach[17, 18]. While both studies propose cell identity markers, and indicate the presence of multiple fibroblast clusters, the data stem from low number of fibroblasts, and results are not comprehensively validated on protein level. We hypothesize that a very detailed analysis of arterial fibroblasts would improve definition of fibroblast identity markers and detailed insight into fibroblast heterogeneity.

In the current study, we therefore investigated the fibroblast transcriptional landscape using scRNA-seq of fibroblast-enriched fractions from healthy murine adventitia. Fibroblast heterogeneity, and pseudotime differentiation trajectories were analyzed in-depth by bioinformatic analyses, such as Potential of Heat-diffusion for Affinity-based Transition Embedding (PHATE). The identified fibroblast identity and cluster markers were validated extensively on RNA and protein level using bulk-, and single cell sequencing, flow cytometry and immunohistochemistry of murine and human healthy and atherosclerotic arteries. We provide support for regulation of fibroblast heterogeneity in CVD, as cardiovascular risk factors differentially affected fibroblast cluster expansion in aged and hypercholesteremic mice *in vivo*, cluster gene signatures harbored a significant number of genes with a known GWAS to CVD and were associated with human atherosclerotic plaque traits. Together, this study provides a detailed fingerprint of arterial fibroblasts in health and CVD.

Methods

Full methods can be found in the online data supplement.

Mouse models

All mouse experiments were approved by the regulatory authority of the Maastricht University Medical Centre and performed in compliance with the Dutch governmental guidelines and Directive 2010/63/EU of the European Parliament on the protection of animals used for scientific purposes. C57BL/6J mice (male, N=8 per pool, 3-4 pools, 8-12 weeks old) were used as healthy controls. Aged C57BL/6J mice (male, N=5 per pool, 3-4 pools, 72 weeks old) were obtained form Charles river and used to study the effect of aging. Male low-density lipoprotein receptor deficient mice (*Ldlr* KO) were fed chow (controls) or high-cholesterol diet (HCD, 0.25%, 824171, Tecnilab-BMI) for 16 weeks (n=15 per pool for single-cell sequencing, n=5 per pool, 3 pools for flow cytometry, 28-30 weeks old). *Ldlr* KO mice originated from Jaxx and were bred in Maastricht for < 15 generations. Pdgfrα-CreERT2-Rosa26-tdTomato and Myh11-CreERT2 eYFP were intraperitonially injected with Tamoxifen (200mg/kg) for three consecutive days, to induce TdTomato expression. Mice were euthanized with an overdose pentobarbital (100mg/kg) injected intraperitoneally.

Flow cytometry and cell sorting

Adventitia of the thoracic aorta (ranging from the aortic root until the diaphragm (Supplemental Video S1)) was carefully microscopically dissociated from the underlaying medial layer and collected in ice-cold PBS. Adventitial tissue of C57BL/6J or *Ldlr* KO mice was enzymatically digested for 15 minutes at 37°C using collagenase B (0.00284g/ml), pronase (0.01g/ml) and DNAse (0.1mg/ml). Living, DAPI-, ICAM2- and CD45- cells were sorted in case of 8 week old C57BL/6J mice or DAPI- cells for *Ldlr* KO.

Adventitial cells isolated originating from either young C57BL/6J mice (8 weeks, male), aged C57BL/6J mice (72 weeks, male), Ldlr KO mice on chow or high cholesterol diet for 16 weeks were used for protein validation. After FC receptor blocking, cells were stained with the following antibodies: CD45, Cdh5/VE-cadherin, Transgelin (TGLN), Platelet derived growth factor alpha (PDGFRA), CD55, CXCL14, and Lysyl oxidase (LOX), live/dead fixable cell stain. In case of CXCL14, the antibody was labelled using a PE/Cy7 conjugation kit. For intracellular stainings (Transgelin, CXCL14 and LOX), fix & perm cell permeabilization kit was used. Data analysis was performed with BD FACS Diva software.

Immunohistochemical stainings

Murine tissue was fixed in 1% paraformaldehyde overnight, paraffin-embedded, and serially sectioned (4µm). For stainings, only sections that had mature media (determined by elastin fiber presence) were used. Tissue sections were stained for the following proteins: SMOC2, PDGFRA, FBLN1, LUMICAN, CCL11, DPEP1, MAC3, CD55, CXCL14, LOX, COL1A1, and total collagen. Images were analyzed either with Qupath (v0.2.0-m8) or Leica Qwin software.

Human sample analysis

Human tissue collection was part of the Maastricht Pathology Tissue Collection (MPTC) and further storage and use of the tissue was in line with the Dutch Code for Proper Secondary use of Human Tissue and the local Medical Ethical Committee (protocol number 16-4-181). This code (https://www.federa.org/codes-conduct) entails an opt-out arrangement and hence tissues were not used in case of objection. The applicability of this code for this study was approved by the Maastricht University hospital (MUMC) local Medical Ethical Committees. Human studies conducted by Li et al.[19] and Wirka et al.[13] are approved by Institutional Review Board at Baylor College of Medicine and Stanford University Institutional Review Board, respectively, and follow the guidelines of the Declaration of Helsinki. Written informed consent was provided by all participants or the organ donors' legal representatives before enrollment. Carotid samples were collected either through autopsy (N=10), carotid endarterectomy procedure (N=63 from 43 patients), from the opposite site of the plaque

(N=10) or during aortic bypass surgery (N=10). Library preparation, RNA extraction, data processing, normalization and additional information concerning plaque traits have been described in great detail elsewhere [20, 21]. Human carotid and aorta single cell sequencing data was retrieved from data repositories and analyzed according to published methods.[13, 19]

Murine Single-cell sequencing

After cell count number and viability check with trypan blue (>85%), a total of ~16.000 CD45-/ICAM2- cells of C57BL/6J mice (N=8) and ~15.000 cells of *Ldlr* KO mice (N=13 for HCD group and N=15 for chow group) were loaded on a chromium 10X genomics controller (V2). Libraries were synthesized and sequenced using Illumina HiSeq4000. Cell and gene number per sample can be found in Supplemental Tables 1 and 2.

Single cell sequencing analysis

Raw sequencing data were processed using CellRanger (v2.1.1 for C57BL/6J mice and v3.0.2 for *Ldlr* KO mice) and analyzed using R and Seurat R package (v.2.3 for C57BL/6J mice and v3.2.3 for *Ldlr* KO mice), and G:profiler[22] for gene ontology analysis of biological processes. Pseudotime analysis were done with PHATE dimension reduction[23], RNA velocyto[24] and Monocle (v.2.10.1)[25]. Full details of analysis can be found in the online data supplement.

Enrichment analysis

DEGs from full trajectories (F1, F2, F3, F4, N = 216; F5, F6, F7, N = 235; F8, F9, N = 317) were intersected with 1) GWAD CAD-associated genes, and 2) Human aorta fibroblasts DEGs originating from the study by Li et al[19]. Hypergeometric testing was used to evaluate the statistical significance of the overlap between trajectory genes and CAD or fibroblast genes. Mouse genes were converted to human genes by biomaRt R package (v2.50.1)[26].

Data availability

Data is deposited (GSE196395) and may be inspected on a web-based interface (Plaqview.com)[27]. Count matrices and code are available upon reasonable request.

Results

ScRNA-seq yields a seven-marker signature differentially regulated in fibroblasts compared to other cells in murine healthy vasculature

The adventitia of the thoracic aorta from 8 healthy male C57Bl/6J mice was collected and pooled for isolation of DAPI-, $CD45^-$, intercellular adhesion molecule 2 $(ICAM2)^-$ cells to to exclude immune and endothelial cells and enrich for the viable, mesenchymal population prior to C analysis (Supplemental Figure S1A-C, Supplemental Video S1). This approach allowed in depth analysis of adventitial mesenchymal cells. In total, 5700 cells passed single cell RNA quality control after removal of low-quality cells (< 1500 genes, >15% mitochondrial reads), and potential doublets (UMI count > 15,000) (Supplemental Tables S1 and S2, Figure 1A-C). Firstly, *in silico* selection of mesenchymal cells was done, based on *Pdgfrβ* expression (Supplemental Figure S1A). Subsequently, annotation of the identified clusters was based on previously published markers for mural cells (Myosin heavy chain 11 (*Myh11*), Transgelin (*Tagln*), Alpha actin (*Acta2*), and calponin (*Cnn1*)) and fibroblasts (*Col1a1, Col1a2* Matrix metalloproteinase 2 (*Mmp2*), and Stem cell antigen-1 (*Sca-1/Ly6a*)[16]). These markers confirmed the presence of both fibroblasts and mural cells in healthy mouse adventitia (Figure 1D-E). The absence of macrophage (*Cd68*), endothelial cell (Platelet endothelial cell adhesion molecule-1 (*Pecam1*)), neuron (RNA binding protein, fox-1 homolog 3 (*Rbfox3*)), and adipocyte (Adiponectin (*Adipoq*)) markers confirmed the purity of our sorting strategy (Supplemental Table S3). Differential gene expression analysis comparing fibroblast and mural cell populations revealed distinct expression profiles for both cell types (Figure 1F). Subsequent gene ontology (GO) enrichment analysis based on differentially expressed genes returned terms including ‘extracellular matrix’ and ‘contractile fiber’ corresponding to fibroblast and mural cell populations, respectively (Supplemental Figure S1D-E).

Notably, many of the commonly proposed fibroblast markers from literature, including vimentin (VIM), matrix metalloproteinase-2 (MMP2), CD90, Sca-1 and Fibroblast Activation Protein (FAP), were not able to fully differentiate between fibroblasts and mural cells, as evidenced by RNA expression in pericytes and smooth muscle cells in three other single cell RNA datasets (Supplemental Figure 2A-B). Despite RNA levels being higher in fibroblasts than mural cells, protein co-expression with TAGLN+ smooth muscle cells was observed in healthy human and murine aorta (Figure 1G-I, Supplemental Figure 2C-E). Thus, we next assessed genes differentially expressed between fibroblasts and mural cells to create a fibroblast-specific transcriptional signature. Differential gene expression (DEG) analysis provided twelve markers preferentially expressed in adventitial fibroblasts (Figure 1J). Enrichment of seven of these markers (Platelet derived growth factor alpha (*Pdgfra*), Dipeptidase 1 (*Dpep1*), SPARC Related Modular Calcium Binding 2 (*Smoc2*), Collagen 14 alpha 1 (*Col14a1*), Fibulin 1 (*Fbln1*), Lumican (*Lum*) and C-C Motif Chemokine Ligand 11 (*Ccl11*)) for mesenchymal fibroblasts remained after validation in two other available scRNA-seq datasets [18, 28] (Supplemental Figure S1F-G). Taken together, seven fibroblast markers (*Pdgfra, Lum, Smoc2, Col14a1, Fbln1, Dpep1, and Ccl11*) selected from our dataset were also expressed in fibroblasts and/or mesenchymal cells in two other datasets comprising healthy murine vasculature and a database including multiple murine organs.

We next validated the fibroblast signature at the protein level using immunohistochemistry and confirmed adventitial localization in healthy mice and expression in spindle-like cells, resembling known fibroblast morphology for all markers, except CCL11. We used the following vascular beds: aortic root (AR), brachiocephalic artery (BCA), ascending aorta (Asc.A), thoracic aorta (Th.A), abdominal aorta (Abd.A) and carotid artery (CA) (Figure 2). PDGFRA and DPEP1 expression was specifically located in the adventitia across all arteries (Figure 2A-B), while LUM, SMOC2, COL14A1, and FBLN1 also showed expression in the media (Figure 2C-F). In case of the latter, it is in accordance with the recent detection of LUM+ myofibroblast-like cells [12, 13, 29]. Negative controls can be observed in Supplemental Figure S3A. Importantly, flow cytometry confirmed that PDGFRA expression was largely similar across various vascular beds (Figure 2G). CCL11 was undetectable in aortic roots (Supplemental Figure S3B-C), concordant with gene expression analyses in heart and aorta from the Tabula Muris consortium [30] (Supplemental Figure S1G).
Moreover, by making use of aorta tissue from smooth muscle cell myosin heavy chain 11 (*Myh11*) reporter mice, and *Pdgfra* reporter mice, we were able to show very limited overlap between *Pdgfra* and *Myh11* (Supplemental Figure S3D-E). This confirmed the highly selective nature of *Pdgfra*, prompting its use in further studies to delineate fibroblast distribution across arteries and heterogeneity.

Trajectory inference analysis predicts the cellular dynamics of fibroblasts in healthy murine adventitia

The single-cell RNA-sequencing analysis not only supported the existence of two distinct cell types, but also suggested heterogeneity within the fibroblast population in a healthy, basal state (Figure 3A). To characterize the cellular dynamics underlying fibroblast heterogeneity, we applied Potential of Heat-diffusion for Affinity-based Trajectory Embedding (PHATE) dimensionality reduction analysis to the dataset to predict differentiation state. PHATE reduction is developed for optimal preservation of patterns in data structure such as continual progressions, branches and clusters, arising due to underlying biological processes, like differentiation[23]. PHATE previously uncovered trajectories, that were undiscoverable by other methods[23]. Subsequent clustering and visualization of data revealed multiple trajectories suggestive of a continuous distinct fibroblast subtypes present in the arterial wall (Figure 3B). Expression of stem cell marker *Sca-1/Ly6a*[31] in most (96.5%) fibroblasts, as shown in Figure 1F, supports the cellular differentiation potential of these cells. Interestingly, one of the three trajectories showed higher *Sca-1/Ly6a* expression throughout the whole trajectory (Supplemental Figure S4A), while end-point clusters of the other two trajectories did not. PHATE analysis did not predict any *Sca-1* expressing fibroblasts to be differentiating into SMCs of the healthy murine adventitia (Supplemental Figure S4B). To

exclude that these trajectories were a result of differences in proliferation, protein synthesis or an artefact related to cell damage, the expression of proliferation markers, and ribosomal and mitochondrial genes, respectively, were investigated. Near absent expression of proliferation markers *Mki67, Cdk1, Cdk2* and *Cenpf*, and uniformly low expression of mitochondrial and ribosomal reads among all clusters was shown (Supplemental Figure S4C-F).

We next mapped RNA velocities[24] onto the PHATE visualization. RNA velocity is estimated based on the proportions of spliced versus unspliced transcripts, allowing for prediction of future cell transcriptional state. In agreement with PHATE analysis, vectors pointing outwards toward branch extremities suggested the differentiation direction of three main trajectories (Figure 3C). Application of Monocle, a third trajectory inference tool[25] further supported the presence of identified trajectories (Supplemental Figure S4G). The inference of the trajectory analysis was that all three trajectories originated from one or more clusters in the center (F1, F5 or F8), hence the possibility of a precursor population was further investigated. Gene signatures for each of these center clusters were constructed (Supplemental Table S4) and the resulting signature scores were presented in violin plots to suggest the origin of the three trajectories (Supplemental Figure S5). This analysis implied that the differential expression of the F1 signature in clusters F2, F3, and F4 supported F1 as the origin of this trajectory (Trajectory 1). The F1 origin of F10 and F11 is likely, but differential expression of the F1 signature was less clear. Similarly, signature analysis suggested F5 as the likely origin of the F6-F7 (Trajectory 2) and F12 trajectories. F8 was inferred to be the likely origin of trajectory 3 given the observed enrichment of its signature in F9.

Furthermore, the observed pattern was not a dataset specific phenomenon, as PHATE analysis of 840 “non-immune” adventitial cells in the dataset by Gu *et al.* [18] also revealed three comparable differentiation trajectories (Figure 3D), supporting the results of our trajectory analysis. Expression of DEGs from the PHATE trajectories originating from the Gu dataset were also confined to three individual trajectories in our own PHATE analysis data (Figure 3E) demonstrating the reproducibility of our findings.

The DEGs in our dataset were further analyzed to investigate possible biological traits associated with the observed trajectories. GO term analysis of DEGs identified in the distal, most differentiated clusters (i.e. F4, F7, F9) of the three trajectories revealed differential annotation of gene ontology terms, and thus potentially different functions (Figure 3F). Trajectories 2 and 3 demonstrated expression of genes involved in extracellular matrix production. Trajectory 1 showed enrichment for terms involved in vasculature development and nucleotide sugar metabolism, trajectory 2 for cholesterol metabolism and antigen presentation and trajectory 3 for response and signaling upon growth factors, and collagen fibril organization. Together, the analysis supports a continuity of phenotype is apparent in adventitial fibroblasts, where most differentiated clusters have differential functional annotations.

Fibroblast clusters validated in healthy murine vasculature

Genes selectively marking the most differentiated cluster of each fibroblast trajectory were identified for validation at the protein level, i.e. F4, F7 and F9 for trajectory 1 through 3 respectively (Supplemental Figure S6). Candidates were selected based on reported expression in fibroblasts, cellular function related to the trajectory GO terms, gene function shown in animal studies, genome-wide associations to be related to known fibroblast functions, and/or processes involved in vascular disease, availability of antibodies for immunohistochemistry and flow cytometry, and/or preferential membrane expression. As an indicator of the most differentiated cluster in trajectory 1, complement decay-accelerating factor (*Cd55*) (Figure 4A) is involved in complement activation and a whole-body KO mouse presented with a protective phenotype against atherosclerosis [32, 33]. The marker representing trajectory 2, chemokine ligand 14 (*Cxcl14*) (Figure 4A) is involved in immune regulation and immune cell migration. [34] Lastly, the marker representing trajectory 3, Lysyl oxidase (*Lox*) is involved in the crosslinking and stabilization of extracellular matrix [35] (Figure 4A). All three

markers (CD55, CXCL14 and LOX) located to the adventitia in healthy murine aortic roots, brachiocephalic arteries, carotid arteries and abdominal aorta, and co-localized with fibroblast marker PDGFRA (Figure 4B-C, Supplemental Figure S7A-B). Flow cytometric analysis showed adventitial protein expression of all three markers in fibroblasts in a variety of vascular beds isolated from healthy C57BL/6J mice (Figure 4D-E). Important to note is that the observed percentages of each end-stage cluster in the thoracic aorta are similar to cluster percentages obtained from our scRNA-seq data (Supplemental Table S5). CD55+ and CXCL14+ fibroblasts are similarly present between arteries, while the frequency of LOX+ fibroblasts varies. All clusters show different distributions within the same artery. These data validate the location, PDGFRA colocalization, frequency and protein expression of key markers for clusters representing each trajectory using two independent techniques.

Cardiovascular risk factors differentially regulate fibroblast clusters

We next queried if the inferred trajectories would be involved in cardiovascular disease, and/or regulated by known CV risk factors. Indeed, we showed that DEGs from all three trajectories were significantly enriched in genes with a single nucleotide polymorphism related to coronary artery disease (Supplemental Table S6). Interestingly, mainly DEGs in CXCL14+ trajectory, showed a highly significant enrichment and the involved DEGs could be linked to the GO terms of this trajectory, e.g. lipid metabolism and inflammation[3, 36]. Thus, we studied if changes in the environment, such as in cardiovascular disease, differentially affected the most differentiated fibroblast clusters in each trajectory. The cardiovascular risk factors, ageing and mild dyslipidemia, initiate early vascular changes and predispose to atherosclerosis, the main cause of cardiovascular disease [37]. To assess the response to these early vascular changes, we used flow cytometry to dissect changes in CD55+, CXCL14+ and LOX+ fibroblasts between young and aged mice, and between normolipidemic wildtype mice and low-density lipoprotein receptor deficient (*Ldlr* KO) mice on a chow diet to induce mild hypercholesterolemia. Interestingly, fibroblast clusters were differentially altered upon ageing and lipidemia. Ageing preferentially increased CD55+ PDGFRA+ and CXCL14+ PDGFRA+ cell fractions, while mild dyslipidemia in *Ldlr* KO mice only increased the LOX+ PDGFRA+ cell fraction, representing the fibrosis-associated trajectory (Figure 5A-B Supplemental Table S7), suggesting the context-dependent importance of the inferred trajectories in progression of disease.

To interrogate whether these changes have functional relevance, we analyzed adventitial area, collagen and inflammatory cell accumulation. LOX is mainly involved in crosslinking immature collagen,[38] and analysis of both mature collagen type I presence and Sirius Red analysis revealed an increase in mature collagen in adventitia from *Ldlr* KO mice (Figure 5C and 5E, and Supplemental Figure S8A, respectively). Notably, the arteries in *Ldlr* KO or aged mice on chow did not show changes in adventitial area, or the major vascular cell populations (Figure 5C-E, Supplemental Table S8), or any sign of atherosclerotic plaque development compared to C57Bl/6J, as expected in only mild hypercholesterolemia and ageing (Figure 5C-D). Immune cell infiltration did not associate with CD55+ or CXCL14+ fibroblasts in ageing. Yet, CXCL14+ fibroblasts, also predicted to act in matrix metabolism, emerged simultaneously as adventitial collagen accumulation in ageing. Hence, the functional changes coinciding with an increase of LOX+ or CXCL14+ fibroblasts precede overt inflammatory, vascular disease.

Atherosclerosis-relevance of murine fibroblast clusters and trajectories

The differential regulation by early vascular changes, prompted us to study the response of adventitial fibroblast clusters to atherosclerosis using scRNA-seq transcriptomics of the adventitia in mild and severe hypercholesterolemic *Ldlr* KO mice. In chow fed mice, 4800 adventitial cells passed quality control and in HCD fed mice, almost 8000 adventitial cells passed the quality control (Supplemental Tables S1 and S2). All expected major cell types in adventitia were identified, with sub-clustering of the identified fibroblast population revealing seven distinct clusters (Figure 6A-B, Supplemental Figure S8B-C). Of note, fibroblast Ly6a/Sca-1 expression was lower in disease, in line with variation in other datasets

(Supplemental Table S9). PHATE reduction analysis confirmed the presence of trajectories equivalent to the original three trajectories in healthy adventitia (Figure 6C). Expression patterns of *Cd55* and *Cxcl14* each remained confined to a single fibroblast trajectory (Figure 6C). This was to a lesser extent visible for *Lox*. *Lox* was less confined to one trajectory, although still mutually exclusive from cells expressing *Cd55*+ *Cxcl14*+. In line with mRNA expression patterns, protein expression of markers for all three trajectories were visualized in PDGFRA fibroblasts of the adventitia underlying advanced murine plaques (Figure 6D). LOX+ fibroblasts were the least prominent at the protein level in this disease condition. These data imply a role for LOX+ fibroblasts in very early stages of atherogenesis, rather than advanced atherosclerosis.

Interestingly, only CD55+ fibroblasts were observed in the atherosclerotic plaque, indicated by the white arrows, in addition to the adventitial layer (Figure 6D). Intriguingly, this trajectory (cluster 0 and 6) also highly expressed stem cell marker *Sca-1/Ly6a* (Figure 6E) and may represent the most plastic, progenitor-like trajectory. This is in line with our healthy scRNA-seq dataset, where the equivalent trajectory highly expressed *Sca-1/Ly6a*. Other groups have already shown that SCA-1 positive cells have the capacity to contribute to neointima formation upon vascular injury[39, 40], yet it remains to be defined if these cells were of fibroblast, MC, or other origin. Our data shed new light on a possible role of specific fibroblast trajectories therein.

Fibroblast clusters are present in atherosclerotic human vasculature

To address the relevance of our murine fibroblast trajectories in human vasculature, we used specimens from carotid anastomosis during aortic bypass surgeries and carotid artery specimens acquired from the opposite side of the culprit plaques during carotid endarterectomy. Both specimens have the advantage that the adventitia is still attached to the vessel wall, allowing investigation of the trajectories in very early stage atherosclerotic human adventitia. Healthy specimens are almost impossible to retrieve the western population, as even asymptomatic patients present with the earliest signs of intimal thickening (IT)[41]. This precludes the use of completely healthy arteries, as we obtained from mice. Nevertheless, all cluster markers representing the three trajectories could be observed in the adventitia of both surgical specimens (Figure 7A, Supplemental Figure S9A), ensuring biological relevance of our identified clusters in human vasculature. In addition, in IT specimens obtained through autopsy from patients without CV symptoms, clusters could also be observed in the adventitia (Supplemental Figure 9B). Moreover, spatial location might be of importance for function. In human intimal thickening sections CD55+ fibroblasts were often observed on the border of the adventitia and media, while CXCL14+ and LOX+ trajectories were more observed surrounding the blood vessels in the adventitia.

To further confirm the presence of trajectories in human vasculature with early signs of disease, we obtained aorta scRNA-seq data from elderly individuals (median age 62) including all arterial wall layers[19]. As these subjects presented with a history of smoking (n=2), diabetes mellitus (n=1), or hypertension (n=1), aortae morphology is expected to show early sign of disease. After selection of the fibroblasts in the dataset, we performed PHATE analysis to assess the presence of trajectories. Also in human aorta with early atherosclerosis, trajectories could be observed that were transcriptionally divergent, although to a lesser extent than in young, healthy mouse adventitia (Figure 7B). Our murine cluster markers were expressed in human aorta fibroblasts, while only *CXCL14* was strictly confined to one human trajectories (Figure 7C). As this is a simplified view based on one marker gene, we tested if the compete gene set differentially expressed by each murine trajectory was significantly enriched in human fibroblasts. Important to note is that genes of the murine trajectories were indeed significantly enriched in the human fibroblasts (Supplemental Table S10). Together these data support human relevance of the observed fibroblast heterogeneity in mice.

We additionally confirm presence of the fibroblast clusters in advanced human atherosclerotic plaques of symptomatic patients undergoing carotid endarterectomy. Protein expression of each cluster marker was confirmed in adventitial PDGFRA+ fibroblasts, but

also in the advanced plaque itself (Figure 7D-E) both on the adventitial as well as the luminal side. Additionally, we correlated differentially expressed genes by murine *CD55*+, *CXCL14*+ and *LOX*+ fibroblasts (46, 32, and 23 genes, respectively) to human plaque traits[21]. The traits were quantified in histology sections adjacent to the segment used for transcriptomics. The distribution of the individual correlations for all genes in a particular fibroblast cluster is shown in Figure 7F. Mostly genes of LOX+ fibroblasts were shown to negatively correlate with detrimental plaque traits, such as plaque size, necrotic core and inflammatory macrophages (Figure 7F). These data suggest differential regulation and/or functions of fibroblast clusters representing the trajectories in human atherosclerosis, as we observed in mice.

Discussion

In this study, we identified arterial fibroblast cell type marker *Pdgfra* and *Dpep1* as most robust, and unveiled pseudotime trajectories of CD55+, CXCL14+ and LOX+ fibroblasts on RNA and protein level across five independent RNA datasets and using histology of five different murine and human arteries. We provide biological implications of these fibroblast clusters in disease in mice and humans: 1) CV risk factors and concomitant environmental triggers drive differential cluster distribution and associate with adventitial fibrosis; 2) Ageing regulated adventitial CD55+ and CXCl14+ fibroblast expansion, and collagen accumulation; 3) mild hypercholesterolemia stimulated LOX+ fibroblast expansion and adventitial fibrosis preceding atherosclerosis; 4) Fibroblast trajectories are present in human adventitia and plaques of symptomatic patients, 5) Fibroblast trajectory genes differentially associated with human plaque traits and were enriched in GWAS genes, suggesting functional implication in human disease development. Together, these findings demonstrate a functional role for adventitial fibroblast trajectories, which could be of interest in disease progression and thus targeted treatments.

The identified arterial fibroblast cell type signature is of importance to the field to accurately distinguish arterial fibroblasts from other vascular cells, as expression of traditional fibroblast markers (e.g. COL1A1/2, VIMENTIN, CD90, S100-A4, FAP, and DCN) is generally not restricted to fibroblasts as shown here and by others[11]. Despite extensive *in silico* validation in three other single-cell transcriptomics datasets in healthy vasculature, protein validation only supported adventitial specificity of PDGFRA and DPEP1 across vascular beds, whereas LUM, COL14A1, SMOC2, and FBLN1 were additionally expressed in the media. Presumably, markers are shared with medial smooth muscle cells, in line with recent identification of LUM as marker for dedifferentiated SMCs in disease[13]. This is important information, as LUM has been coined as a fibroblast marker in several single-cell studies with mouse, primate, and human arteries, yet without proper validation[17, 42, 43]. Alternatively, differences in embryonic origin between arteries could explain medial expression, in line with different embryonic origins of SMC[44]. The embryonic origin of adventitial fibroblasts in most arteries is not fully clear but is important to understand homeostasis and response to injury. Previous work showed that the neural crest was the origin of coronary artery adventitia[44], yet others excluded this origin in ascending aorta and support second heart field.[45] Instead, dedifferentiation of medial SCA-1/LY6A+ SMCs was shown[28], which offers a third explanation of ambiguity of our fibroblast signature. Trans differentiation between SMCs and fibroblasts in atherosclerosis is seemingly bi-directional[13, 46]. Our data indeed suggest variation in embryonic origin and/or trans differentiation across arteries. Whether this also explains variation in trajectory dominance across arteries remains to be resolved using dual lineage reporter mice. Overall, the adventitial-specific location of PDGFRA and DPEP1 across arteries and absent medial co-localization of PDGFRA and SMC marker MYH11 in lineage reporter mice, support specificity of this marker for arterial fibroblasts across healthy arteries, recommending this marker for future studies. A *Pdgfra* lineage tracing mouse would give insight in the location and distribution of fibroblasts healthy but also diseased adventitia. In atherosclerosis, this would also reveal fate of adventitial fibroblasts, which is of interest considering evidence of endothelial or smooth muscle cell

origin of fibroblast-like cells in plaques[13, 14]. These studies are however beyond the scope of the current study.

The importance of adventitial cells in vascular pathology has been studied over the years, specifically focusing on the Ly6aSca-1+ progenitor population as a whole[6, 46], as recently reviewed by Jolly et al.[1] This population includes both mesenchymal and immune progenitors as shown by targeted phenotyping, and by our own data. Using our unbiased approach to phenotype adventitial mesenchymal cells, we show that the *Pdgfra/Dpep1* fibroblast population includes *Ly6a/Sca-1*+ cells, but also *Ly6a/Sca-1* low or negative cells. Moreover, *Ly6a/Sca-1*+ fibroblast decrease in presence upon atherosclerosis, which might be a result of differentiation upon disease induction. On the other hand, we show that adventitial LY6A/SCA-1+ cells include more than fibroblasts alone. Hence, *Ly6a/Sca-1*+ cells do not fully recapitulate PDGFRA+ cells, a concept which is important for interpretation of results. The CD55+ trajectory cells express high level and frequency of *Ly6a/Sca*-1 and its function may thus most closely resemble published reports on adventitial *Ly6a/Sca-1*+ progenitor cells.

Biological implications of CD55+, CXCL14+ and LOX+ fibroblasts may be gained from their differential association and response to experimentally changed cardiovascular risk factors, i.e. age and serum lipids, and enrichment of genes with a GWAS to CAD. CD55+ fibroblasts were linked to vascular development and were increased upon aging. In endometrioid tumor, CD55 was found to be essential in self-renewal[47], which would be in line with our findings of coinciding expression of Sca-1 and CD55+ trajectory. Increasing the presence of the CD55+ trajectory might induce rejuvenation, through increased plasticity and potential to adapt to pathogenesis. In addition, CD55 has a role in complement regulation, and its stimulation may trigger detrimental vascular inflammation. This is in line with observation in atherosclerosis, where whole-body CD55 deficiency was shown to be atheroprotective in ApoE KO mice[32]. As CD55 is one gene of 46, skewing the entire trajectory would probably not reflect the effect of the single CD55 knock-out. CXCL14+ trajectory also expanded upon vascular aging. GO terms of the CXCL14+ trajectory included extracellular matrix organization, and antigen presentation, amongst others. In vascular ageing, we only observed an association of this trajectory with fibrosis, likely owing to the four collagen genes in this trajectory (*Col4a1, 5a3, 6a3, 15a1*). This is in line with a positive effect on fibrotic gene expression and proliferation of fibroblasts[48], and the absent effect of *Cxcl14* KO on immune cell recruitment in homeostasis[49]. However, upon a stronger pro-inflammatory milieu, like in overt atherosclerosis, this aspect of CXCL14 function may be important. Indeed, this trajectory was also detected in advanced plaques by histology and single cell sequencing. In line, *Cxcl14* expression was enhanced in mouse primary macrophages by oxidized LDL, and peptide immune therapy diminished serum CXCL14 levels and murine atherosclerosis[50]. Although attributed to macrophages so far, conditional deletion of *Cxcl14* using existing *Pdgfra*- or future *Dpep1*-Cre models may unveil the effect of CXCL14+ fibroblasts in atherogenesis.

While CD55+ and CXCL14+ fibroblasts expanded upon vascular aging, expansion of LOX+ fibroblasts was triggered only by a mild increase in serum cholesterol. The early rise of LOX+ fibroblasts coinciding with adventitial collagen deposition prior to disease development, possibly implies a regenerative role for LOX+ fibroblasts to strengthen the vessel upon a lipid challenge. Higher total LOX protein abundance in plaques was associated with plaque stability, while, seemingly opposing, *Lox* mRNA levels predicted the risk of myocardial infarction.[51] Although these effects of LOX have thus far been attributed to SMCs[52], future studies are warranted to challenge this view. Together, we foresee skewing trajectories towards more favorable subsets through conditional knock-out models, which might have great relevance for atherogenesis and vascular aging, like the improved balance between lung myogenic and lipofibroblasts spurring lung fibrosis[53]. Likewise, dampening pro-inflammatory fibroblasts or promoting matrix-fibroblasts may be beneficial for plaque progression. An interesting addition to this is that lipid-lowering medications that are prescribed on a regular basis, e.g. statins, could already influence fibroblast abundance and

matrix production[54]. Studies investigating the beneficial lipid-lowering effect vs. the negative effect on fibroblast presence and functions are warranted.

The current study has some limitations. Current single-cell sequencing technology has limited sequencing depth and is therefore biased towards genes with high expression levels. Nevertheless, the resolution at single cell level has already provided new insights in arterial biology in health and disease, as well as corroborated existing ones [2, 18, 28, 55]. Enrichment of mesenchymal cells yielded sufficiently high fibroblast cell number to reveal transcriptional regulation of small subsets of cells, which remained obscured in two "atlas" datasets with smaller fibroblast numbers [17, 18]. While their approach had the advantage to study all cells simultaneously, as well a cell-cell communication, our approach prevents analysis of cell-cell communication. Moreover, the lack of healthy, human adventitial single cell sequencing datasets prevents direct comparison of the adventitial fibroblast transcriptome and subsets between mouse and human. Another limitation pertains to a causal implication of the observed association between the fibroblast trajectories and human plaque characteristics. Future studies with conditional depletion of trajectory genes or their master regulators in *Pdgfra+/Dpep1+* fibroblasts would give us insight how targeted elimination of fibroblast trajectories would impact atherogenesis.

In conclusion, PDGFRA specifically marks arterial fibroblasts across arterial beds, with CD55+, CXCL14+ and LOX+ fibroblasts showing differential association to human cardiovascular disease and response to cardiovascular risk factors. Together, these new insights will aid to determine the role of fibroblasts in disease progression and future targeted treatment plans.

Author contributions

Conceptualization: J.C.S., A.H.B, K.V.K., I.R.M. Methodology: K.V.K., I.R.M., R.J.H.A.T., S.E.J.A., R.W.S., R.S.T. A.H.B. and J.C.S., Formal analysis: K.V.K., I.R.M., R.J.H.A.T., S.E.J.A., R.W.S., R.S.T., and J.C.S., Investigation: K.V.K., I.R.M., R.J.H.A.T., S.E.J.A., R.W.S., R.S.T., C.K., H.J., S.M., D.K., M.J.G., L.T., J.L., P.G., Resources: R.D., P.R., Y.L., H.N., J.R.W.K., L.J.S., Y.H.S., B.M.E.M., E.A.L.B., N.C.H., and R.K., Writing- Original draft: J.C.S. and K.V.K., Writing- Review & Editing: K.V.K., I.R.M., A.H.B., J.C.S., Funding acquisition, J.C.S.; Supervision: A.H.B., J.C.S.

Acknowledgements

The authors thank T. Abud, J. Debets, C. Dinjens, P. Leenders and E. Wijnands for their technical assistance, and Gary K. Owens for providing *Myh11*-CreERT2 eYFP tissue sections. Flow assisted cell sorting was done with support from the QMRI Flow Cytometry and cell sorting facility, University of Edinburgh, and at the Flow Cytometry Facility at RWTH Aachen.

Funding

This work was funded by the Netherlands organization for scientific research (NWO) VIDI (#91718364) and ASPASIA grant (015.013.064) to J.C.S., a Wellcome Trust Senior Research Fellowship in Clinical Science (ref. 219542/Z/19/Z) to N.C.H., DFG/TRR219 M-05 to H.N., ERC advanced grant (VASCMIR) and British Heart foundation Chair of Translational Cardiovascular Sciences to A.H.B.

Conflict of interest

The authors declare no conflicts of interest.

Figure legends

Figure 1. Single-cell RNA sequencing reveals fibroblast transcriptional signature for healthy murine aortic adventitia

A. T-distributed stochastic neighbour embedding (t-SNE) plot of single cell sequencing data derived from CD45-/ICAM2-/PDGFRβ+ adventitial cells from pool of 9 young C57Bl6 mice. **B.** Mitochondrial signature of fibroblasts and mural cells (MC) post-filtering, **C.** Ribosomal signature of fibroblasts and MC post-filtering, **D**. Expression of mural cell (MC) markers (*Myh11, Acta2, Tgln, Cnn1*), and **E.** traditional fibroblast markers (*Col1α1, Col1α2, Ly6a, Mmp2)* projected on tSNE plot from figure 1D shows cell type annotation, **F.** Heatmap of differentially expressed genes (DEGs) in fibroblasts and MC. Immunohistochemical staining of SMC marker Tgln (red) with traditional fibroblast markers (green) in mouse, **G.** Vimentin (VIM), **H.** CD90 and **I.** human aorta (VIM) **J.** Violin plots of twelve genes differentially expressed in fibroblasts compared to mural cells (MC).

Figure 2. Validation of fibroblast signature across multiple vascular beds

Representative immunohistochemical staining of proposed fibroblast markers, **A.** Platelet derived growth factor alpha (PDGFRA), **B.** Dipeptidase 1 (DPEP1), **C.** Collagen 14 alpha 1 (COL14A1), **D.** Lumican (LUM), **E.** Sparc-related modular calcium binding 2 (SMOC2), and **F.** Fibulin 1 (FBLN1), in healthy murine C57BL/6J Aortic roots (AR), Brachiocephalic artery (BCA), Ascending aorta (Asc.A), Thoracic aorta (Th.A), Abdominal aorta (Abd.A) and Carotid artery (CA) n=10). Nuclei in blue, fibroblast makers in green. L, indicates Lumen, M indicates Media, and A indicates Adventitia. **G**. PDGFRA+ frequencies of live CD45-/CDH5+/TAGLN+ adventitial cells across C57BL/6J arteries (thoracic aorta (Th.A), Abdominal aorta (Abd.A), Brachiocephalic artery (BCA), Carotid artery (CA), and Femoral artery (FA)), analyzed by flow cytometry (n=4 pools of 5 mice each, 20 mice total). Statistical analysis was performed using Kruskal-Wallis test, with Dunn's post-hoc test (G). Results are shown as mean ± SEM. * $p<0.05$ vs Th. A.

Figure 3. Trajectory analysis shows distinct phenotypes of fibroblasts in healthy murine adventitia

A. tSNE plot of fibroblasts originating from figure 1D**. B.** PHATE pseudotime trajectory analysis of fibroblasts from figure 1D depicting twelve clusters differentiating along several trajectory paths. **C.** RNA velocity analysis on PHATE data from figure 3B, arrows are indicating directionality. **D.** Data was validated by PHATE analysis on an independent dataset from Gu et al.[18] (840 cells from healthy murine adventitia) showing three trajectories**. E.** Feature plots show expression of three differentially expressed genes in trajectories from Gu dataset on Gu PHATE map, and their expression in three trajectories of the PHATE map of our dataset (van Kuijk), **F.** Dot plot of the gene ontology (GO) terms from the most differentiated clusters (F4, F7, F9) representing each trajectory 1-3 respectively with most relevant GO terms in bold.

Figure 4. Fibroblast clusters representing three trajectories can be identified on transcriptional and protein level in healthy murine adventitia

A. Projection of clusters markers representing the three trajectories *Cd55*, *Cxcl14* and *Lox* on PHATE plot from figure 3A, **B.** Immunohistochemical staining of CD55, CXCL14 and LOX in aortic roots of healthy C57Bl/6J mice (n=10). Pan-fibroblast marker PDGFRA in green and fibroblast trajectory markers in red. Yellow areas indicate double-positive cells for PDGFRA and cluster- marker (marked with arrows in 63X magnification). L, indicates Lumen, M indicates Media, A indicates Adventitia. **C.** Quantification of double positive cells for each cluster in aortic roots of figure 4B. **D.** Flow cytometry gating strategy of each fibroblast cluster. **E.** Fibroblast clusters in adventitia of Thoracic aorta (Th.A), Abdominal aorta (Ab.A), Brachiocephalic artery (BCA), Carotid artery (CA), and Femoral artery (FA) assessed by flow cytometry in 4 pools of 5 mice, 20 mice in total. Statistical analyses were performed using one-way ANOVA with Bonferroni post-hoc test (C) or two-way ANOVA with Tukey post-hoc

test (E). All results show mean ± SEM. * p<0.05, ** P<0.01, or *** P<0.001 vs. *CD55*+ fibroblasts in same artery; # P<0.05 or ### P<0.001 vs. same cluster in Th. A.

Figure 5. Fibroblast clusters representing three trajectories are differentially regulated upon cardiovascular risk factors

A. Flow cytometry analysis of fibroblast clusters representing three trajectories in thoracic aorta adventitia from young or aged C57BL/6J mice, 12 or 72 weeks old respectively. (N=4 pools of young mice, 9 mice per pool (36 mice total) vs. N=3 pools of aged mice, 4-5 mice per pools (14 mice total), respectively). Data are depicted as mean ± SEM. **B.** Flow cytometry analysis of fibroblast clusters representing trajectories in adventitia from low density lipoprotein receptor knock-out (*Ldlr* KO) mice on chow diet vs. healthy C57BL/6J mice. (N=3 pools, 4 mice per pool (12 mice total) vs. N=3 pools, 6 mice per pool (18 mice total), respectively). Data are depicted as mean ± SEM. **C.** Representative images of Collagen type I, **D.** MAC3 immunohistochemical stainings, and **E.** quantification of adventitial area, collagen type I and MAC3+ cells in adventitia of young, *Ldlr* KO and aged mice (11, 10, and 9 mice per group, respectively). Positive cells or area are observed in brown, nuclei in blue. Statistical analyses were performed using two-way ANOVA (A-B) or one-way ANOVA (E), with Bonferroni post-hoc test. All results show mean ± SEM. **p<0.0032, ****p<0.0001, ##p<0.0060, ###p<0.0006.

Figure 6. Fibroblast cluster markers representing three trajectories are still observed in atherosclerosis, while LOX+ fibroblasts reduced in presence

A. Unsupervised clustering of single-cell sequencing data from *Ldlr* KO mice on chow or 16 weeks of high cholesterol diet (HCD). Results are visualized by Uniform Manifold Approximation and Projection (UMAP), colors represent individual clusters, **B.** PHATE visualization of fibroblasts originating from the dataset in Figure 6A, colors represent individual clusters. **C.** Cluster markers projected on fibroblast PHATE plot of figure 6B, representing trajectory 1 using *Cd55*, trajectory 2 using *Cxcl14*, and trajectory 3 using *Lox*. **D**. Protein expression of each cluster marker visualized by immunohistochemistry in aortic roots from *Ldlr* KO mice after 16 weeks high cholesterol diet. Pan-fibroblast marker in green and fibroblast cluster markers in red. Yellow areas indicate double-positive cells for pan fibroblast and cluster marker (Marked with arrows). L, indicates Lumen, P indicates Plaque, A indicates Adventitia. **E.** *Sca-1/Ly6a* mRNA expression visualized on PHATE map, originating from Figure 6B, depicting fibroblast clusters.

Figure 7. Fibroblast trajectories correlate differentially to human atherosclerotic plaque phenotype

A. Immunohistochemical stainings of CD55+fibroblasts, CXCL14+fibroblasts, and LOX+fibroblasts representing trajectory 1-3 respectively in human intimal thickening specimens collected through autopsy, accompanied with corresponding H&E, Pan-fibroblast marker in green and fibroblast trajectory markers in red. Yellow areas indicate double-positive cells for pan fibroblast and cluster marker. M indicates Media, A indicates Adventitia. **B.** PHATE analysis of fibroblasts in scRNA-seq dataset by Li et al. [19]. showing four clusters. **C.** Fibroblast cluster markers representing the trajectories from mouse scRNA-seq data extrapolated to feature plots of human control data. Immunohistochemical stainings of CD55+fibroblasts, CXCL14+fibroblasts, and LOX+ fibroblasts representing trajectory 1-3 respectively in advanced human atherosclerotic plaques, showing the adventitial side (**D**) and the luminal side (**E**), accompanied by the corresponding H&E. Pan-fibroblast marker in green and fibroblast trajectory markers in red. Yellow areas indicate double-positive cells for pan fibroblast and cluster marker. M, indicates Media, P indicates Plaque, A indicates Adventitia. **F.** Violin plots depicting correlations of all genes differentially expressed by each fibroblast trajectory with plaque traits in 43 human carotid plaque segments. Significant violin plots ($p < 0.05$) were denoted with a black border. Significance was assessed by positive and negative correlations and the unbalance thereof, which was defined as the sum of positive

correlations minus the sum of absolute values of negative correlations. Furthermore, correlation skewness was compared between trajectory genes and a random gene set containing a similar number of genes. The permutation test was performed 100,000 times and the p-value is the frequency of the random gene sets that have higher correlation skewness than the trajectory gene set.

References

1. Jolly AJ, Lu S, Strand KA, Dubner AM, Mutryn MF, Nemenoff RA, Majesky MW, Moulton KS, Weiser-Evans MCM. Heterogeneous subpopulations of adventitial progenitor cells regulate vascular homeostasis and pathological vascular remodeling. *Cardiovasc Res* 2021.
2. van Kuijk K, Kuppe C, Betsholtz C, Vanlandewijck M, Kramann R, Sluimer JC. Heterogeneity and plasticity in healthy and atherosclerotic vasculature explored by single-cell sequencing. *Cardiovasc Res* 2019;**115**:1705-1715.
3. Xie T, Wang Y, Deng N, Huang G, Taghavifar F, Geng Y, Liu N, Kulur V, Yao C, Chen P, Liu Z, Stripp B, Tang J, Liang J, Noble PW, Jiang D. Single-Cell Deconvolution of Fibroblast Heterogeneity in Mouse Pulmonary Fibrosis. *Cell Rep* 2018;**22**:3625-3640.
4. Guerrero-Juarez CF, Dedhia PH, Jin S, Ruiz-Vega R, Ma D, Liu Y, Yamaga K, Shestova O, Gay DL, Yang Z, Kessenbrock K, Nie Q, Pear WS, Cotsarelis G, Plikus MV. Single-cell analysis reveals fibroblast heterogeneity and myeloid-derived adipocyte progenitors in murine skin wounds. *Nat Commun* 2019;**10**:650.
5. Tillie R, van Kuijk K, Sluimer JC. Fibroblasts in atherosclerosis: heterogeneous and plastic participants. *Curr Opin Lipidol* 2020;**31**:273-278.
6. Majesky MW, Dong XR, Hoglund V, Daum G, Mahoney WM, Jr. The adventitia: a progenitor cell niche for the vessel wall. *Cells Tissues Organs* 2012;**195**:73-81.
7. Lee S, Park C, Han JW, Kim JY, Cho K, Kim EJ, Kim S, Lee SJ, Oh SY, Tanaka Y, Park IH, An HJ, Shin CM, Sharma S, Yoon YS. Direct Reprogramming of Human Dermal Fibroblasts Into Endothelial Cells Using ER71/ETV2. *Circ Res* 2017;**120**:848-861.
8. Xiao D, Liu X, Zhang M, Zou M, Deng Q, Sun D, Bian X, Cai Y, Guo Y, Liu S, Li S, Shiang E, Zhong H, Cheng L, Xu H, Jin K, Xiang M. Direct reprogramming of fibroblasts into neural stem cells by single non-neural progenitor transcription factor Ptf1a. *Nat Commun* 2018;**9**:2865.
9. Shi Y, O'Brien JE, Jr., Mannion JD, Morrison RC, Chung W, Fard A, Zalewski A. Remodeling of autologous saphenous vein grafts. The role of perivascular myofibroblasts. *Circulation* 1997;**95**:2684-2693.
10. Li M, Riddle S, Zhang H, D'Alessandro A, Flockton A, Serkova NJ, Hansen KC, Moldvan R, McKeon BA, Frid M, Kumar S, Li H, Liu H, Canovas A, Medrano JF, Thomas MG, Iloska D, Plecita-Hlavata L, Jezek P, Pullamsetti S, Fini MA, El Kasmi KC, Zhang Q, Stenmark KR. Metabolic Reprogramming Regulates the Proliferative and Inflammatory Phenotype of Adventitial Fibroblasts in Pulmonary Hypertension Through the Transcriptional Co-Repressor C-terminal Binding Protein-1. *Circulation* 2016.
11. Kuwabara JT, Tallquist MD. Tracking Adventitial Fibroblast Contribution to Disease: A Review of Current Methods to Identify Resident Fibroblasts. *Arterioscler Thromb Vasc Biol* 2017;**37**:1598-1607.
12. Alencar GF, Owsiany KM, Karnewar S, Sukhavasi K, Mocci G, Nguyen AT, Williams CM, Shamsuzzaman S, Mokry M, Henderson CA, Haskins R, Baylis RA, Finn AV, McNamara CA, Zunder ER, Venkata V, Pasterkamp G, Bjorkegren J, Bekiranov S, Owens GK. Stem Cell Pluripotency Genes Klf4 and Oct4 Regulate Complex SMC Phenotypic Changes Critical in Late-Stage Atherosclerotic Lesion Pathogenesis. *Circulation* 2020;**142**:2045-2059.
13. Wirka RC, Wagh D, Paik DT, Pjanic M, Nguyen T, Miller CL, Kundu R, Nagao M, Coller J, Koyano TK, Fong R, Woo YJ, Liu B, Montgomery SB, Wu JC, Zhu K, Chang R, Alamprese M, Tallquist MD, Kim JB, Quertermous T. Atheroprotective roles of smooth muscle cell phenotypic modulation and the TCF21 disease gene as revealed by single-cell analysis. *Nat Med* 2019;**25**:1280-1289.
14. Evrard SM, Lecce L, Michelis KC, Nomura-Kitabayashi A, Pandey G, Purushothaman KR, d'Escamard V, Li JR, Hadri L, Fujitani K, Moreno PR, Benard L, Rimmele P, Cohain A, Mecham B, Randolph GJ, Nabel EG, Hajjar R, Fuster V, Boehm M,

Kovacic JC. Endothelial to mesenchymal transition is common in atherosclerotic lesions and is associated with plaque instability. *Nat Commun* 2016;**7**:11853.
15. Kramann R, Schneider RK, DiRocco DP, Machado F, Fleig S, Bondzie PA, Henderson JM, Ebert BL, Humphreys BD. Perivascular Gli1+ progenitors are key contributors to injury-induced organ fibrosis. *Cell Stem Cell* 2015;**16**:51-66.
16. Muhl L, Genove G, Leptidis S, Liu J, He L, Mocci G, Sun Y, Gustafsson S, Buyandelger B, Chivukula IV, Segerstolpe A, Raschperger E, Hansson EM, Bjorkegren JLM, Peng XR, Vanlandewijck M, Lendahl U, Betsholtz C. Single-cell analysis uncovers fibroblast heterogeneity and criteria for fibroblast and mural cell identification and discrimination. *Nat Commun* 2020;**11**:3953.
17. Kalluri AS, Vellarikkal SK, Edelman ER, Nguyen L, Subramanian A, Ellinor PT, Regev A, Kathiresan S, Gupta RM. Single-Cell Analysis of the Normal Mouse Aorta Reveals Functionally Distinct Endothelial Cell Populations. *Circulation* 2019;**140**:147-163.
18. Gu W, Ni Z, Tan YQ, Deng J, Zhang SJ, Lv ZC, Wang XJ, Chen T, Zhang Z, Hu Y, Jing ZC, Xu Q. Adventitial Cell Atlas of wt (Wild Type) and ApoE (Apolipoprotein E)-Deficient Mice Defined by Single-Cell RNA Sequencing. *Arterioscler Thromb Vasc Biol* 2019;**39**:1055-1071.
19. Li Y, Ren P, Dawson A, Vasquez HG, Ageedi W, Zhang C, Luo W, Chen R, Li Y, Kim S, Lu HS, Cassis LA, Coselli JS, Daugherty A, Shen YH, LeMaire SA. Single-Cell Transcriptome Analysis Reveals Dynamic Cell Populations and Differential Gene Expression Patterns in Control and Aneurysmal Human Aortic Tissue. *Circulation* 2020;**142**:1374-1388.
20. Jin H, Mees BME, Biessen EAL, Sluimer JC. Transcriptional Sex Dimorphism in Human Atherosclerosis Relates to Plaque Type. *Circ Res* 2021;**129**:1175-1177.
21. Jin H, Goossens P, Juhasz P, Eijgelaar W, Manca M, Karel JMH, Smirnov E, Sikkink C, Mees BME, Waring O, van Kuijk K, Fazzi GE, Gijbels MJJ, Kutmon M, Evelo CTA, Hedin U, Daemen M, Sluimer JC, Matic L, Biessen EAL. Integrative multiomics analysis of human atherosclerosis reveals a serum response factor-driven network associated with intraplaque hemorrhage. *Clin Transl Med* 2021;**11**:e458.
22. Raudvere U, Kolberg L, Kuzmin I, Arak T, Adler P, Peterson H, Vilo J. g:Profiler: a web server for functional enrichment analysis and conversions of gene lists (2019 update). *Nucleic Acids Res* 2019;**47**:W191-W198.
23. Moon KR, van Dijk D, Wang Z, Gigante S, Burkhardt DB, Chen WS, Yim K, Elzen AVD, Hirn MJ, Coifman RR, Ivanova NB, Wolf G, Krishnaswamy S. Visualizing structure and transitions in high-dimensional biological data. *Nat Biotechnol* 2019;**37**:1482-1492.
24. La Manno G, Soldatov R, Zeisel A, Braun E, Hochgerner H, Petukhov V, Lidschreiber K, Kastriti ME, Lonnerberg P, Furlan A, Fan J, Borm LE, Liu Z, van Bruggen D, Guo J, He X, Barker R, Sundstrom E, Castelo-Branco G, Cramer P, Adameyko I, Linnarsson S, Kharchenko PV. RNA velocity of single cells. *Nature* 2018;**560**:494-498.
25. Trapnell C, Cacchiarelli D, Grimsby J, Pokharel P, Li S, Morse M, Lennon NJ, Livak KJ, Mikkelsen TS, Rinn JL. The dynamics and regulators of cell fate decisions are revealed by pseudotemporal ordering of single cells. *Nat Biotechnol* 2014;**32**:381-386.
26. Durinck S, Spellman PT, Birney E, Huber W. Mapping identifiers for the integration of genomic datasets with the R/Bioconductor package biomaRt. *Nat Protoc* 2009;**4**:1184-1191.
27. Ma WF, Hodonsky CJ, Turner AW, Wong D, Song Y, Mosquera JV, Ligay AV, Slenders L, Gancayco C, Pan H, Barrientos NB, Mai D, Alencar GF, Owsiany K, Owens GK, Reilly MP, Li M, Pasterkamp G, Mokry M, van der Laan SW, Khomtchouk BB, Miller CL. Enhanced single-cell RNA-seq workflow reveals coronary artery disease cellular cross-talk and candidate drug targets. *Atherosclerosis* 2022;**340**:12-22.

28. Dobnikar L, Taylor AL, Chappell J, Oldach P, Harman JL, Oerton E, Dzierzak E, Bennett MR, Spivakov M, Jorgensen HF. Disease-relevant transcriptional signatures identified in individual smooth muscle cells from healthy mouse vessels. *Nat Commun* 2018;**9**:4567.
29. Pan H, Xue C, Auerbach BJ, Fan J, Bashore AC, Cui J, Yang DY, Trignano SB, Liu W, Shi J, Ihuegbu CO, Bush EC, Worley J, Vlahos L, Laise P, Solomon RA, Connolly ES, Califano A, Sims PA, Zhang H, Li M, Reilly MP. Single-Cell Genomics Reveals a Novel Cell State During Smooth Muscle Cell Phenotypic Switching and Potential Therapeutic Targets for Atherosclerosis in Mouse and Human. *Circulation* 2020;**142**:2060-2075.
30. Tabula Muris C. Single-cell transcriptomics of 20 mouse organs creates a Tabula Muris. *Nature* 2018;**562**:367-372.
31. Morikawa S, Mabuchi Y, Kubota Y, Nagai Y, Niibe K, Hiratsu E, Suzuki S, Miyauchi-Hara C, Nagoshi N, Sunabori T, Shimmura S, Miyawaki A, Nakagawa T, Suda T, Okano H, Matsuzaki Y. Prospective identification, isolation, and systemic transplantation of multipotent mesenchymal stem cells in murine bone marrow. *J Exp Med* 2009;**206**:2483-2496.
32. Lewis RD, Perry MJ, Guschina IA, Jackson CL, Morgan BP, Hughes TR. CD55 deficiency protects against atherosclerosis in ApoE-deficient mice via C3a modulation of lipid metabolism. *Am J Pathol* 2011;**179**:1601-1607.
33. Dho SH, Lim JC, Kim LK. Beyond the Role of CD55 as a Complement Component. *Immune Netw* 2018;**18**:e11.
34. Lu J, Chatterjee M, Schmid H, Beck S, Gawaz M. CXCL14 as an emerging immune and inflammatory modulator. *J Inflamm (Lond)* 2016;**13**:1.
35. Csiszar K. Lysyl oxidases: a novel multifunctional amine oxidase family. *Prog Nucleic Acid Res Mol Biol* 2001;**70**:1-32.
36. Arellano-Rodriguez M, Zapata-Benavides P, Arellano-Rodriguez NC, Izaguirre-Alvarez JM, Franco-Molina MA, F DEJTDM, Mendoza-Gamboa E, Soto-Dominguez A, Saavedra-Alonso S, Rodriguez-Padilla C. The Inflammatory Process Modulates the Expression and Localization of WT1 in Podocytes Leading to Kidney Damage. *In Vivo* 2021;**35**:3137-3146.
37. Frostegard J. Immunity, atherosclerosis and cardiovascular disease. *BMC Med* 2013;**11**:117.
38. Lucero HA, Kagan HM. Lysyl oxidase: an oxidative enzyme and effector of cell function. *Cell Mol Life Sci* 2006;**63**:2304-2316.
39. Kokkinopoulos I, Wong MM, Potter CMF, Xie Y, Yu B, Warren DT, Nowak WN, Le Bras A, Ni Z, Zhou C, Ruan X, Karamariti E, Hu Y, Zhang L, Xu Q. Adventitial SCA-1(+) Progenitor Cell Gene Sequencing Reveals the Mechanisms of Cell Migration in Response to Hyperlipidemia. *Stem Cell Reports* 2017;**9**:681-696.
40. Tang J, Wang H, Huang X, Li F, Zhu H, Li Y, He L, Zhang H, Pu W, Liu K, Zhao H, Bentzon JF, Yu Y, Ji Y, Nie Y, Tian X, Zhang L, Gao D, Zhou B. Arterial Sca1(+) Vascular Stem Cells Generate De Novo Smooth Muscle for Artery Repair and Regeneration. *Cell Stem Cell* 2020;**26**:81-96 e84.
41. Virmani R, Kolodgie FD, Burke AP, Farb A, Schwartz SM. Lessons from sudden coronary death: a comprehensive morphological classification scheme for atherosclerotic lesions. *Arterioscler Thromb Vasc Biol* 2000;**20**:1262-1275.
42. Zhang W, Zhang S, Yan P, Ren J, Song M, Li J, Lei J, Pan H, Wang S, Ma X, Ma S, Li H, Sun F, Wan H, Li W, Chan P, Zhou Q, Liu GH, Tang F, Qu J. A single-cell transcriptomic landscape of primate arterial aging. *Nat Commun* 2020;**11**:2202.
43. Hu Z, Liu W, Hua X, Chen X, Chang Y, Hu Y, Xu Z, Song J. Single-Cell Transcriptomic Atlas of Different Human Cardiac Arteries Identifies Cell Types Associated With Vascular Physiology. *Arterioscler Thromb Vasc Biol* 2021;**41**:1408-1427.
44. Sawada H, Rateri DL, Moorleghen JJ, Majesky MW, Daugherty A. Smooth Muscle Cells Derived From Second Heart Field and Cardiac Neural Crest Reside in Spatially

Distinct Domains in the Media of the Ascending Aorta-Brief Report. *Arterioscler Thromb Vasc Biol* 2017;**37**:1722-1726.
45. Sawada H, Katsumata Y, Higashi H, Zhang C, Li Y, Morgan S, Lee LH, Singh SA, Chen JZ, Howatt DA, Moorleghen JJ, Franklin MK, Rateri DL, Shen YH, LeMaire SA, Aikawa M, Majesky MW, Lu HS, Daugherty A. Second Heart Field-derived Cells Contribute to Angiotensin II-mediated Ascending Aortopathies. *bioRxiv* 2022:2020.2002.2002.930917.
46. Hu Y, Zhang Z, Torsney E, Afzal AR, Davison F, Metzler B, Xu Q. Abundant progenitor cells in the adventitia contribute to atherosclerosis of vein grafts in ApoE-deficient mice. *J Clin Invest* 2004;**113**:1258-1265.
47. Saygin C, Wiechert A, Rao VS, Alluri R, Connor E, Thiagarajan PS, Hale JS, Li Y, Chumakova A, Jarrar A, Parker Y, Lindner DJ, Nagaraj AB, Kim JJ, DiFeo A, Abdul-Karim FW, Michener C, Rose PG, DeBernardo R, Mahdi H, McCrae KR, Lin F, Lathia JD, Reizes O. CD55 regulates self-renewal and cisplatin resistance in endometrioid tumors. *J Exp Med* 2017;**214**:2715-2732.
48. Li L, Li Q, Wei L, Wang Z, Ma W, Liu F, Shen Y, Zhang S, Zhang X, Li H, Qian Y. Chemokine (C-X-C motif) ligand 14 contributes to lipopolysaccharide-induced fibrogenesis in mouse L929 fibroblasts via modulating PPM1A. *J Cell Biochem* 2019;**120**:13372-13381.
49. Meuter S, Schaerli P, Roos RS, Brandau O, Bosl MR, von Andrian UH, Moser B. Murine CXCL14 is dispensable for dendritic cell function and localization within peripheral tissues. *Mol Cell Biol* 2007;**27**:983-992.
50. Tong W, Duan Y, Yang R, Wang Y, Peng C, Huo Z, Wang G. Foam Cell-Derived CXCL14 Muti-Functionally Promotes Atherogenesis and Is a Potent Therapeutic Target in Atherosclerosis. *J Cardiovasc Transl Res* 2020;**13**:215-224.
51. Ovchinnikova OA, Folkersen L, Persson J, Lindeman JH, Ueland T, Aukrust P, Gavrisheva N, Shlyakhto E, Paulsson-Berne G, Hedin U, Olofsson PS, Hansson GK. The collagen cross-linking enzyme lysyl oxidase is associated with the healing of human atherosclerotic lesions. *J Intern Med* 2014;**276**:525-536.
52. Martinez-Revelles S, Garcia-Redondo AB, Avendano MS, Varona S, Palao T, Orriols M, Roque FR, Fortuno A, Touyz RM, Martinez-Gonzalez J, Salaices M, Rodriguez C, Briones AM. Lysyl Oxidase Induces Vascular Oxidative Stress and Contributes to Arterial Stiffness and Abnormal Elastin Structure in Hypertension: Role of p38MAPK. *Antioxid Redox Signal* 2017;**27**:379-397.
53. El Agha E, Moiseenko A, Kheirollahi V, De Langhe S, Crnkovic S, Kwapiszewska G, Szibor M, Kosanovic D, Schwind F, Schermuly RT, Henneke I, MacKenzie B, Quantius J, Herold S, Ntokou A, Ahlbrecht K, Braun T, Morty RE, Gunther A, Seeger W, Bellusci S. Two-Way Conversion between Lipogenic and Myogenic Fibroblastic Phenotypes Marks the Progression and Resolution of Lung Fibrosis. *Cell Stem Cell* 2017;**20**:261-273 e263.
54. Porter KE, Turner NA, O'Regan DJ, Balmforth AJ, Ball SG. Simvastatin reduces human atrial myofibroblast proliferation independently of cholesterol lowering via inhibition of RhoA. *Cardiovasc Res* 2004;**61**:745-755.
55. Cochain C, Vafadarnejad E, Arampatzi P, Pelisek J, Winkels H, Ley K, Wolf D, Saliba AE, Zernecke A. Single-Cell RNA-Seq Reveals the Transcriptional Landscape and Heterogeneity of Aortic Macrophages in Murine Atherosclerosis. *Circ Res* 2018;**122**:1661-1674.

Figure 1

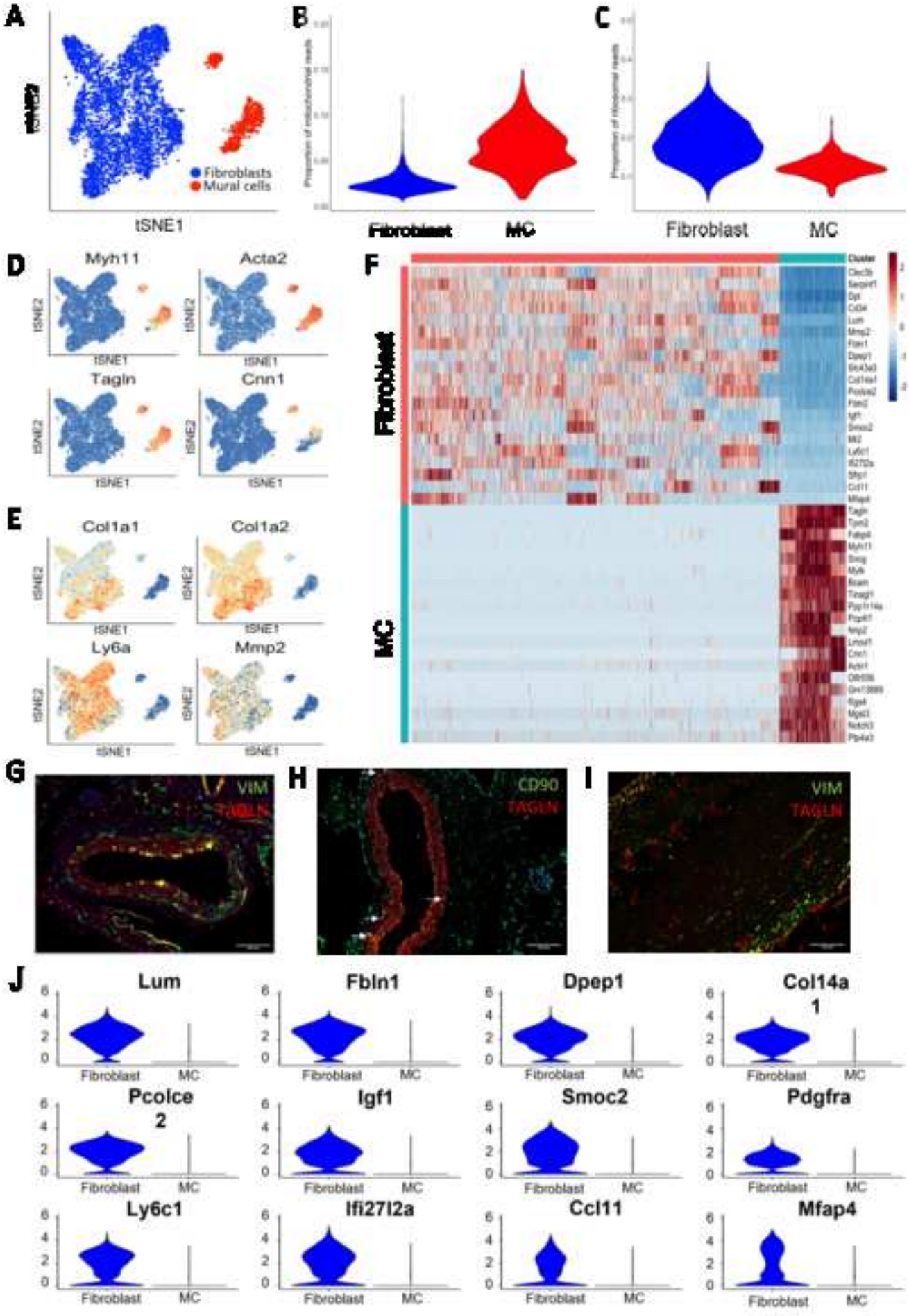

Figure 2

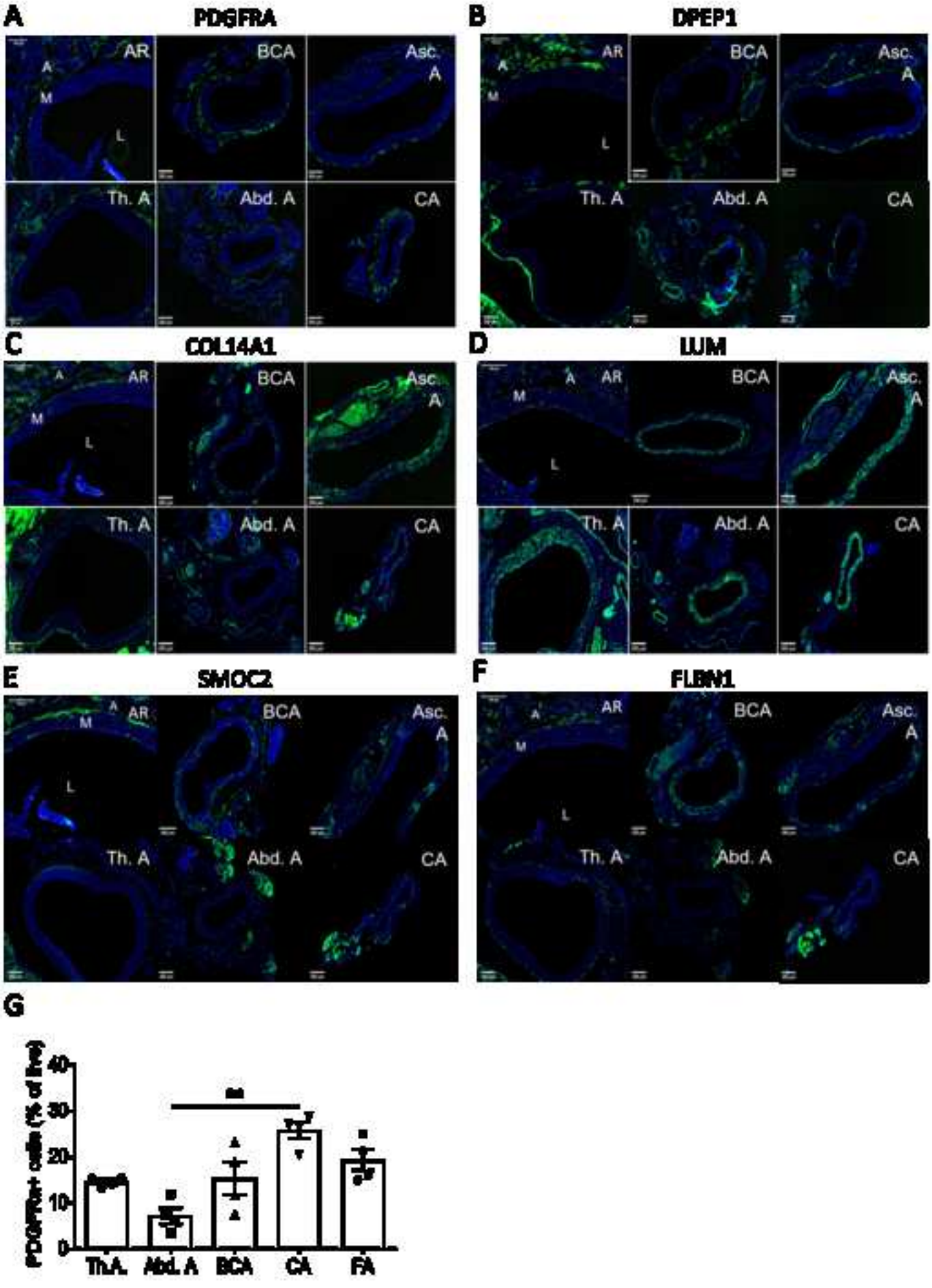

Figure 3

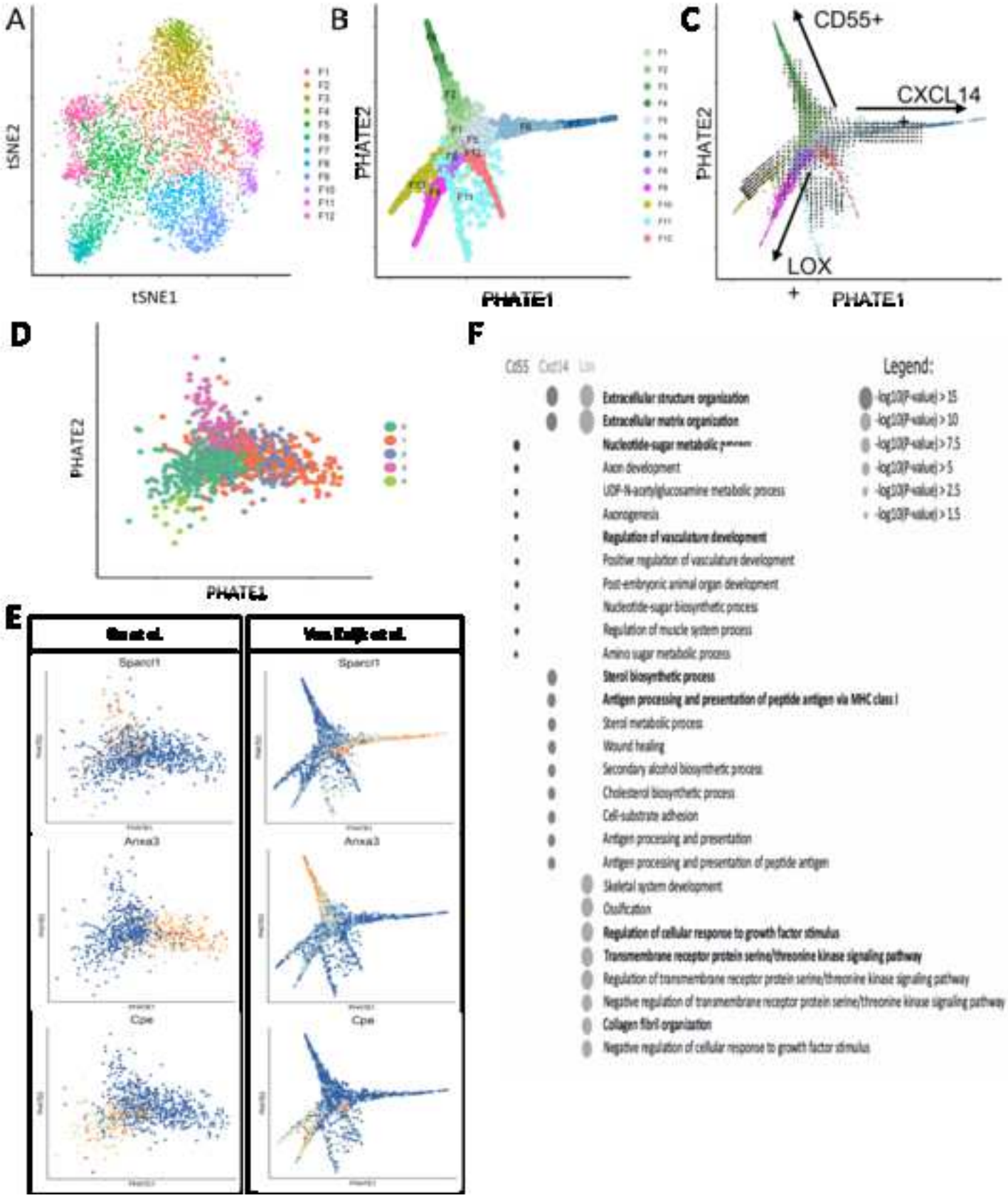

Figure 4

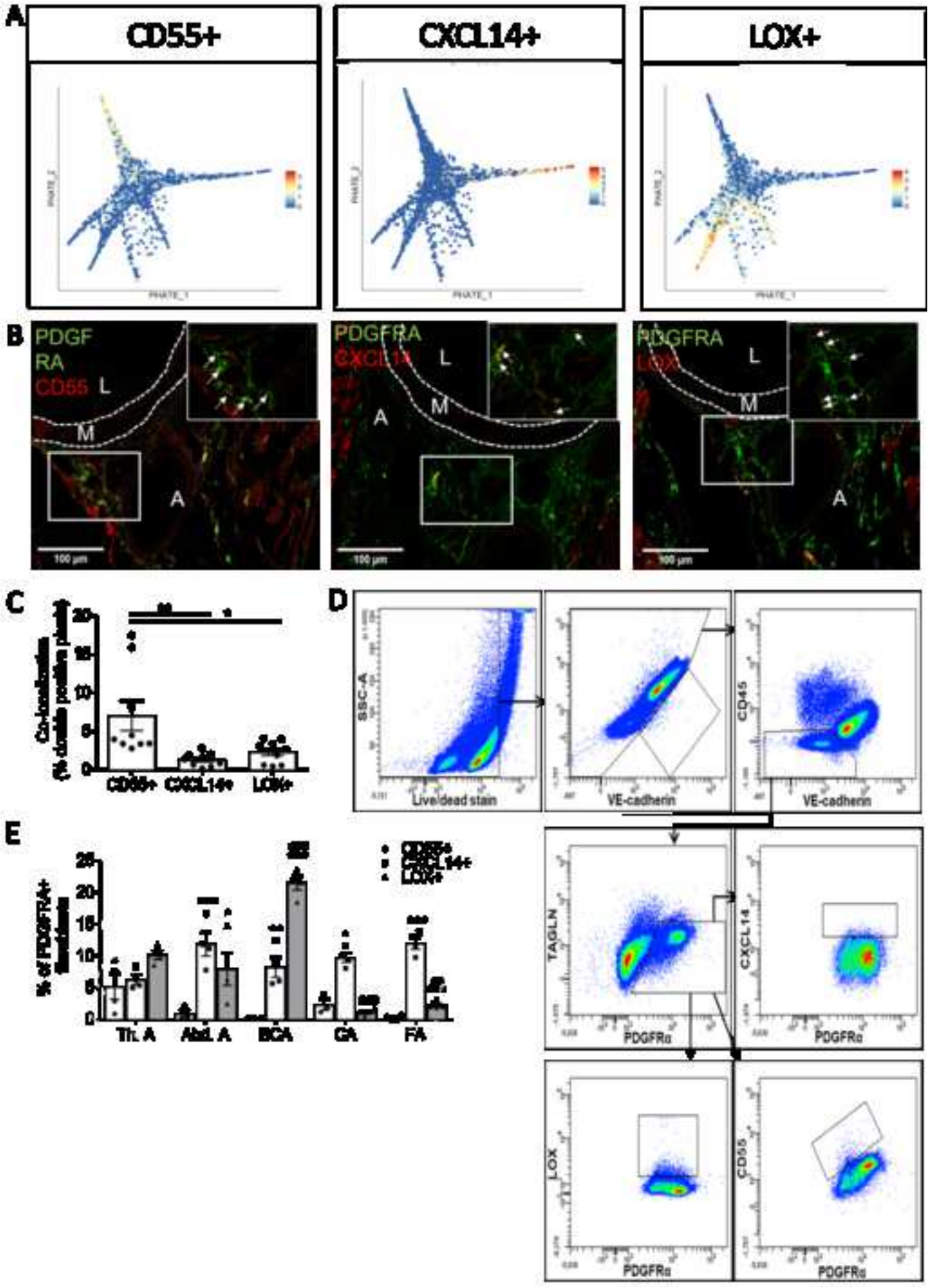

Figure 5

Click here to access/download;Figure(s);Figure 5.tif

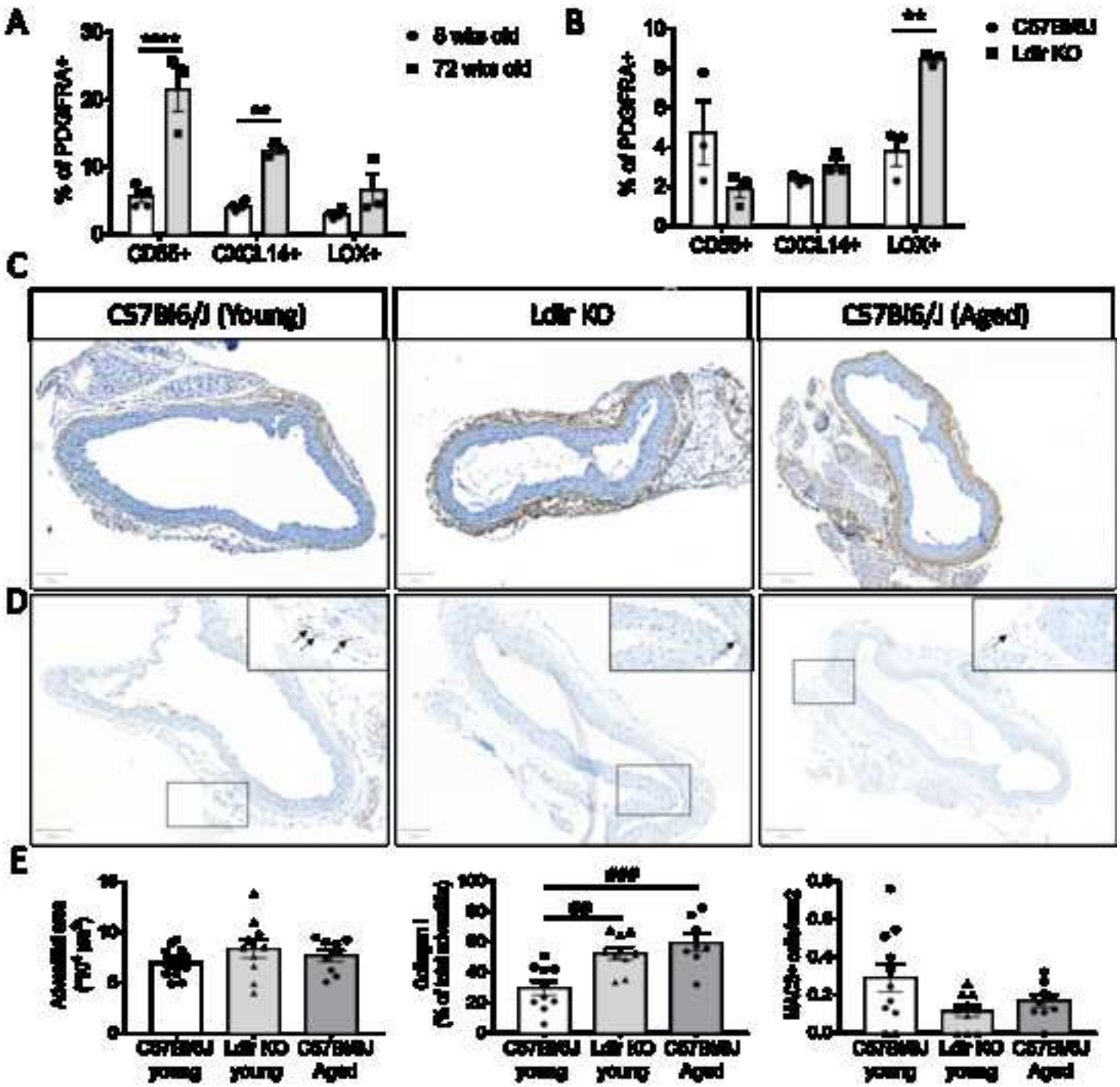

Figure 6

Click here to access/download;Figure(s);Figure 6.tif

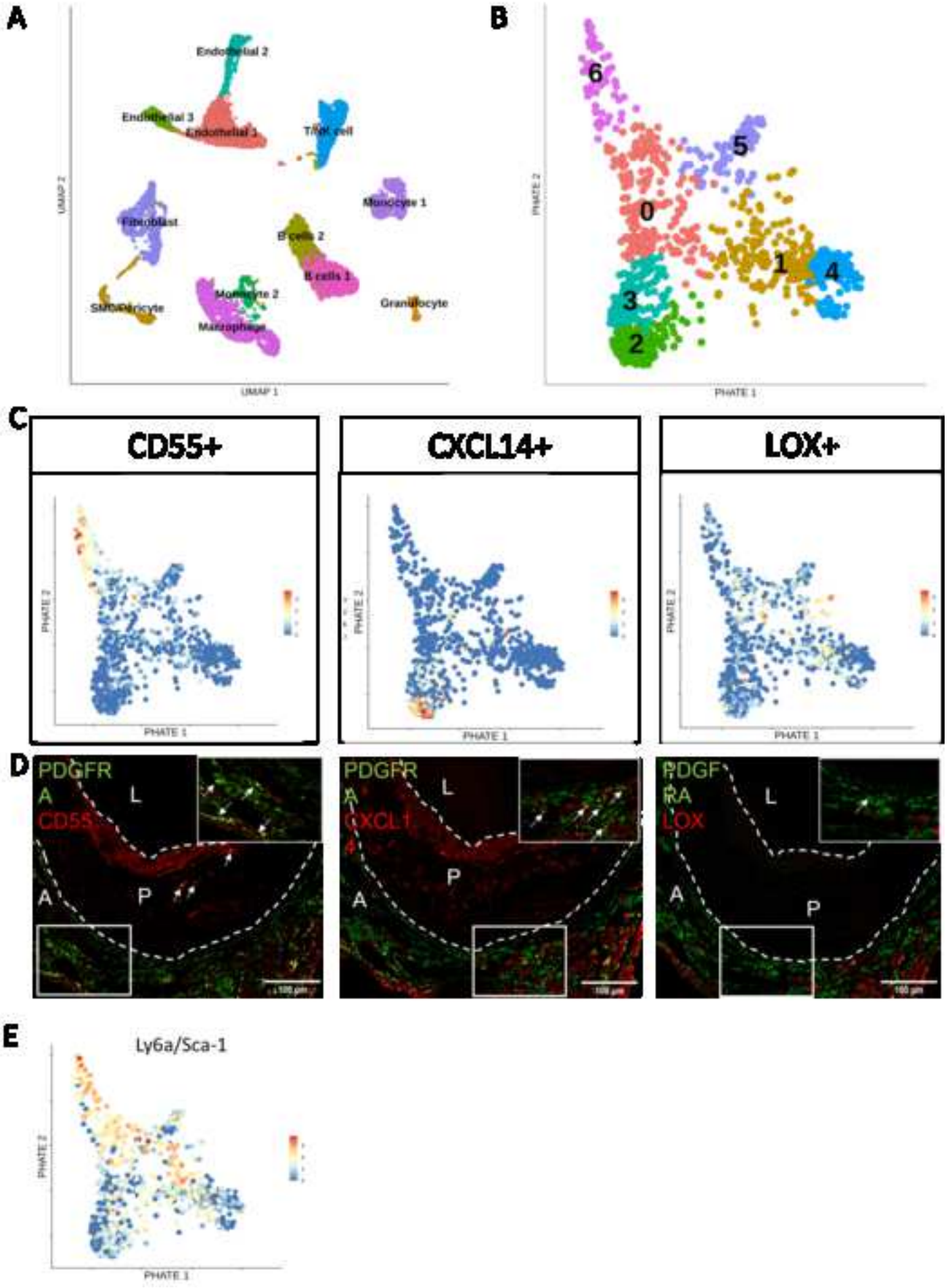

Figure 7

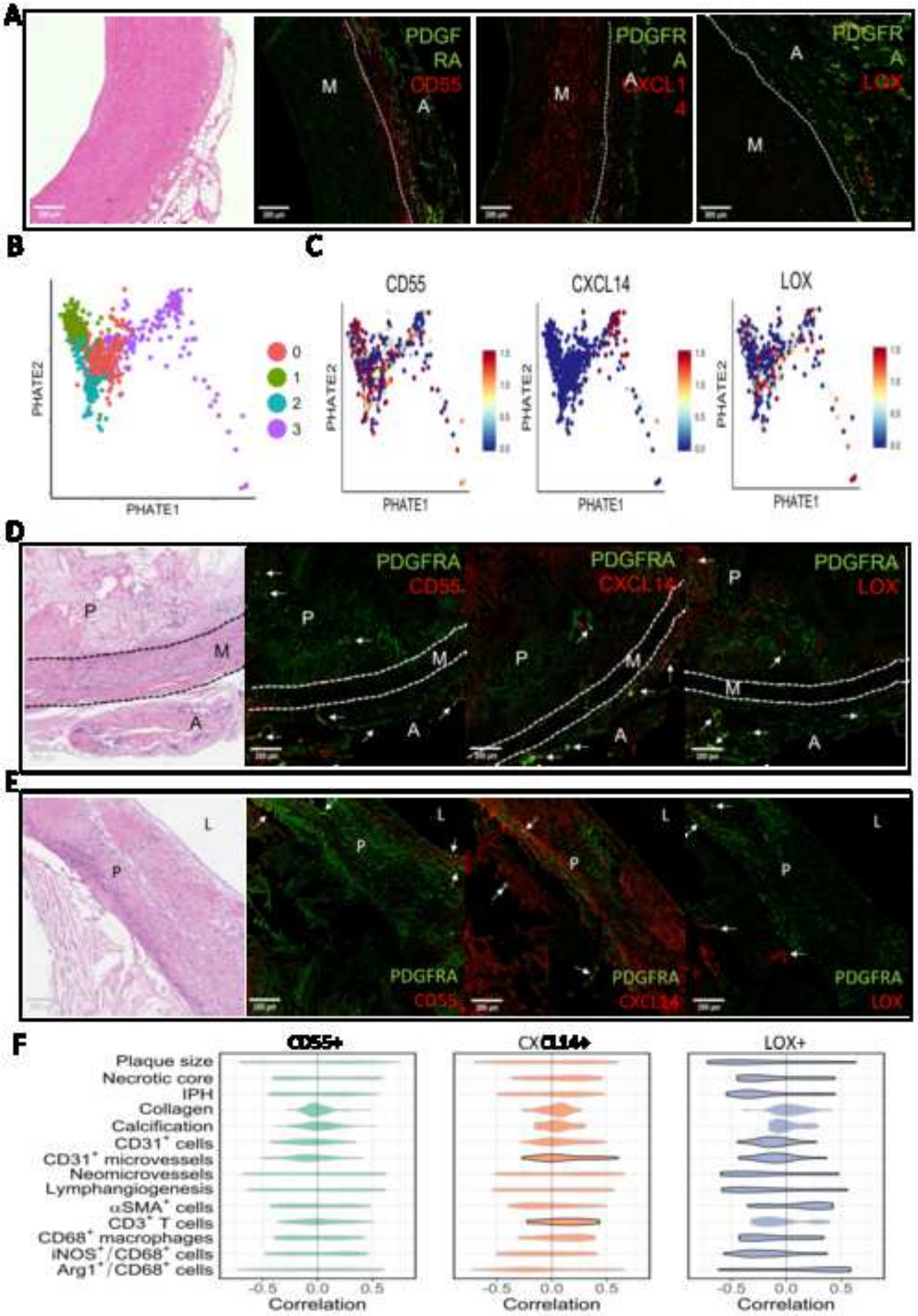

Graphical Abstract

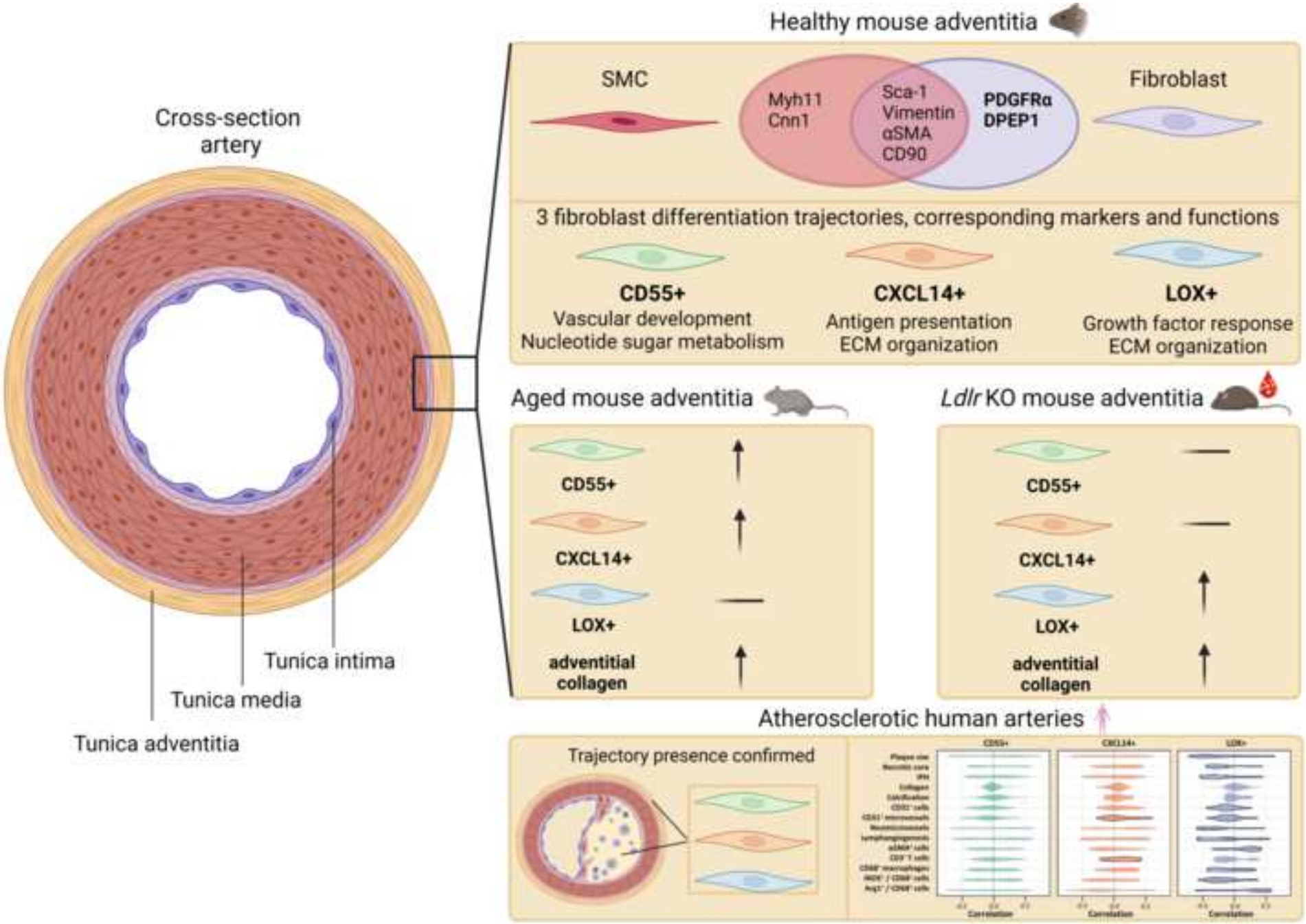

Online data supplement to:

Human and murine fibroblast single cell transcriptomics reveals reveals fibroblast clusters are differentially affected by ageing, and serum cholesterol

Fibroblast clusters in health and disease

van Kuijk K[1,2], McCracken IR[3], Tillie RJHA[1], Asselberghs SEJ[1,4], Kheder DA[1], Muitjens S[1], Jin H[1], Taylor RS[3], Wichers Schreur R[1], Kuppe C[2,5], Dobie R[6], Ramachandran P[6], Gijbels MJ[1,7,8], Temmerman L[1], Kirkwood PM[6], Luyten J[1,4], Li Y[9,10], Noels H[11], Goossens P[1], Wilson-Kanamori JR[5], Schurgers LJ[1,2], Shen YH [9,10], Mees BME[1,4], Biessen EAL[1,11], Henderson NC[5,12], Kramann R[2,4], Baker AH[1,3], Sluimer JC[1,3]

Table of contents:

Supplemental Tables

Supplemental Table S1. Cell counts after quality control as indicated in CellRanger software

Parameter	C57BL/6J (#)	*Ldlr* KO, chow (#)	*Ldlr* KO, 16 weeks HCD (#)
Estimated number of cells	5,701	4,822	7,989
Mean reads/cell	87,456	63,948	47,390
Median genes/cell	2,490	2,359	1,640
Median UMI counts/cell	7,169	6,794	3,545

Supplemental Table S2. Sequencing parameters for 10X Genomics samples

Sequencing	C57BL/6J (%)	*Ldlr* KO, chow (%)	*Ldlr* KO, 16 weeks HCD (%)
Valid barcodes	98.4	96.0	95.8
Reads mapped confidently to transcriptome	66.9	51.6	44.4
Reads mapped confidently to exonic regions	69.3	56.0	48.5
Reads mapped confidently to intronic regions	15.1	30.8	36.0
Reads mapped confidently to intergenic regions	2.8	4.3	5.0
Sequencing saturation	85.4	69.0	65.0

Supplemental Table S3. Expression of markers macrophages, endothelial cells, neurons and adipocytes in C57BL/6J scRNA-seq dataset

Markers	Cells with detected expression (%)
Cd68 (Macrophages)	0.25
Pecam1 (Endothelial cells)	6.13
Rbfox3 (Neurons)	1.45
Adipoq (Adipocytes)	0.50

Supplemental Table S4. Differentially expressed genes (DEGs) in each individual core cluster compared to the other core clusters (F1 vs. F5 vs. F8)

F1 vs. F5 & F8 signature	F5 vs. F1 & F8 signature	F8 vs. F1 & F5 signature
Pla1a	Cxcl12	Mfap4
Gm12840	Gdf10	Col8a1
Ifi205	Steap4	Cilp
Sult1e1	Nrp1	Eln
Lrrn4cl	Ccl11	Angptl1
Ifi204	Clec11a	Fxyd6
Wt1		Itgbl1
Cotl1		Aspn
Efemp1		Sfrp1
		Lox
		Tgfb3
		Cpxm2
		Pdgfrl
		Wisp2
		C1qtnf2
		Fgl2
		Avpr1a
		Pcsk5
		Pmepa1
		Fibin
		Dkk2
		Hmcn2
		Crispld2
		Cpe
		Cdkn1c

Supplemental Table S5. Fibroblast cluster proportions represented as the percentages of the total population of fibroblast.

Cluster	F1	F2	F3	F4	F5	F6	F7	F8	F9	F10	F11	F12
Proportion (%)	16.54	9.26	8.73	3.83	17.21	5.27	3.75	10.60	8.59	3.02	3.24	9.96

Supplemental Table S6. Enrichment of differentially expressed genes of each trajectory in GWAS for coronary artery disease (CAD) expressed as p-value.

GWAS CAD	p-value	Intersected genes
CD55+ Trajectory (F1234)	$3.5*10^{-2}$	IL6R
CXCL14+ Trajectory (F567)	$<5*10^{-6}$	LPL, LOXL1, WT1, SERPINH1, COL6A3
LOX+ Trajectory (F89)	$2*10^{-3}$	TMEM204, GEM, ZEB2

Supplemental Table S7. Blood cholesterol levels of young C57BL/6J mice, aged C57BL/6J mice and *Ldlr* KO mice on chow diet or high cholesterol diet for 16 weeks

Mouse model	Diet	Cholesterol levels (mmol/L)
C57BL/6J (N=36)	Chow (8 wks old)	1.30±0.55
C57BL/6J (N=14)	Chow (72 wks old)	1.28±0.62
Ldlr KO (N=11)	Chow	4.10±2.25
Ldlr KO (N=13)	16 weeks high cholesterol diet	14.23±8.33

Supplemental Table S8. Adventitial cell populations of *Ldlr* KO mice on chow diet vs. normolipidemic C57BL/6J mice, proportional to relevant populations measured by flow cytometry. Values are represented as average from 3 pools, consisting of 3-6 mice.

Mouse model	Endothelial cells (% of living)	Immune cells (% of living, VE-cadherin-)	Smooth muscle cells (% of living, VE-cadherin-,CD45-)	Fibroblasts (% of living, VE-cadherin-,CD45-)	Other (% of living)
C57BL/6J (N=36)	0.2	1.2	3.0	31.0	64.6
Ldlr KO (N=11)	0.8	0.8	3.8	26.5	68.1

Supplemental Table S9. Percentages of Ly6a/Sca-1 expressing fibroblasts in single cell sequencing datasets used in the current manuscript.

Data	Publication	% of fibroblasts expressing Ly6a/Sca-1
Healthy C57BL/6J	This manuscript	94.8
Ldlr KO (Chow)	This manuscript	92.9
Ldlr KO (HCD)	This manuscript	59.3
C57BL/6J	Gu et al. 2019 ATVB	86.0
C57Bl/6	Dobnikar et al. 2018 Nature Communications	43.6

Supplemental Table S10. Enrichment of murine trajectory-specific genes in human fibroblast population originating from dataset by Li et al.

Trajectory	-10log(p-value)
CD55+ Trajectory (F1234)	2.17
CXCL14+ Trajectory (F567)	15.32
LOX+ Trajectory (F89)	21.24

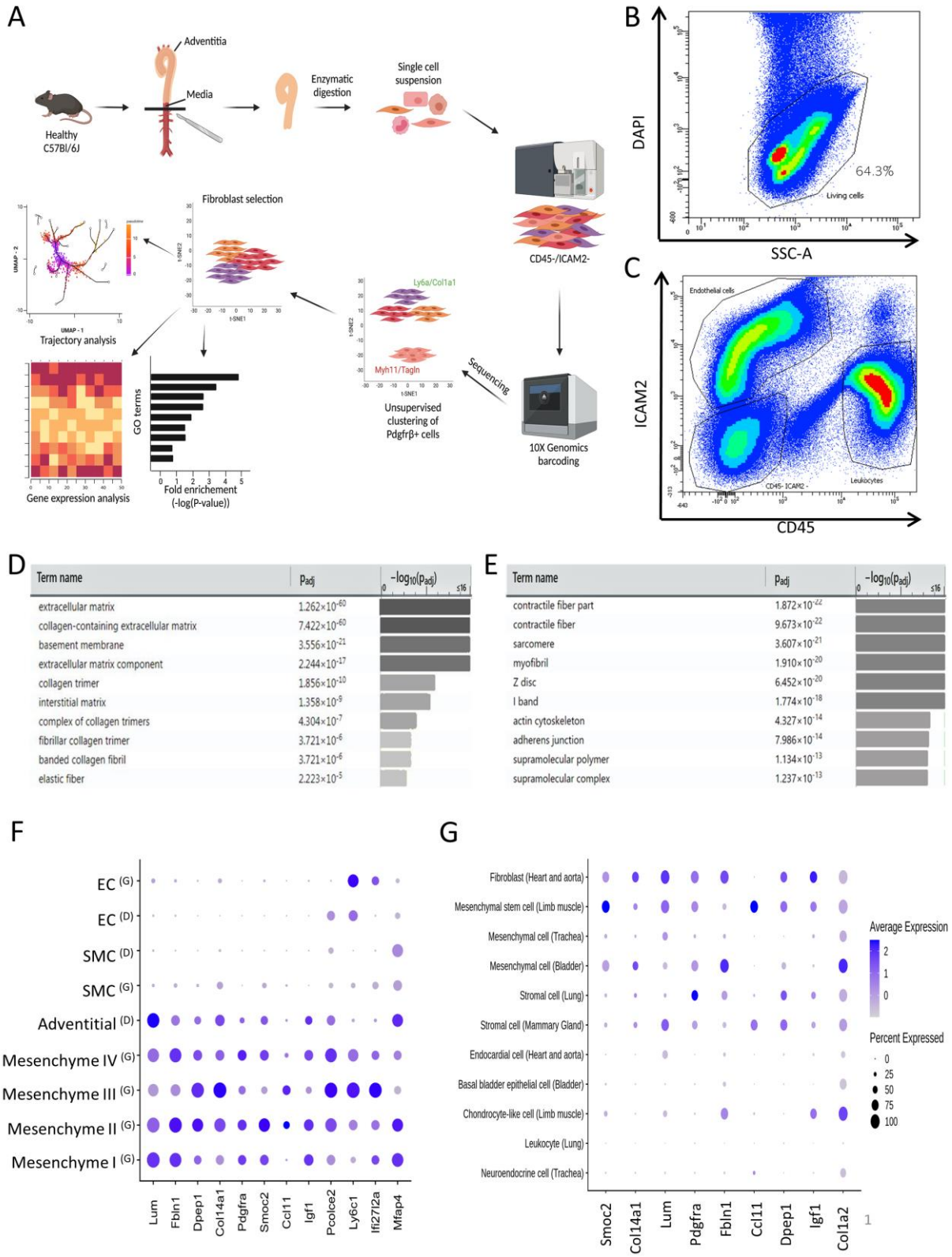

Supplemental figure S1. Fibroblast characterization using single cell sequencing. A. Diagram depicting study approach from tissue isolation from healthy C57Bl/6J mice and further processing, **B.** Selection of living DAPI- cells (64.3%) from pooled adventitial samples of 8 male mice **C.** Flow cytometry gating strategy for selection of CD45-, ICAM2- cells from DAPI- cells (9.7% of living) from figure 1B for scRNA-seq, **D.** Top ten GO-term analysis of cellular processes of fibroblasts, or **E.** MCs. **F**. Dot plot of marker specificity in healthy murine adventitia (G)[56] , and healthy media (D) [57], **G.** Marker validation in mesenchymal and fibroblasts from single cell expression data of Tabula Muris consortium [58]. Annotation of cell types in **F** and **G** is according to the original paper.

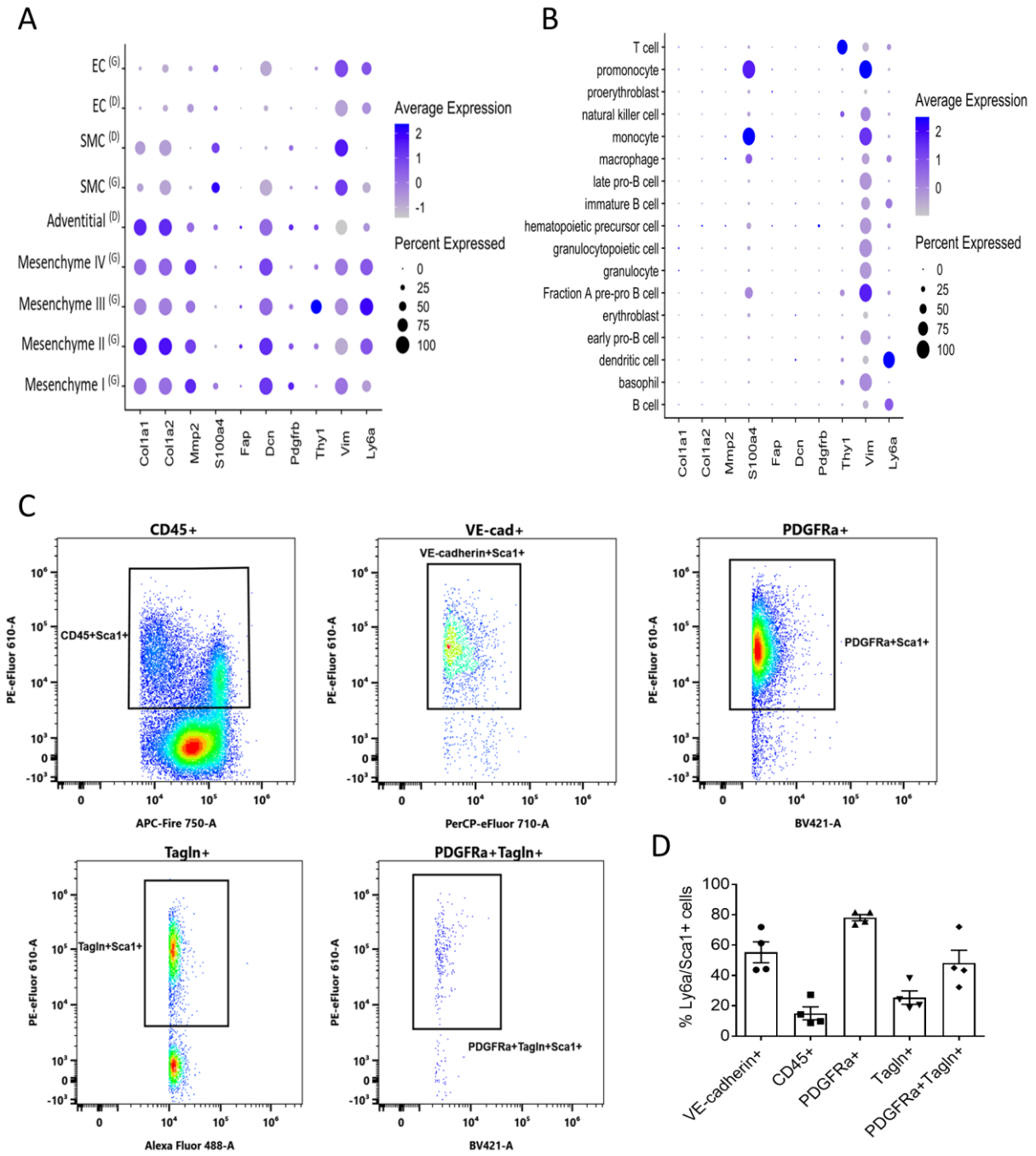

Supplemental figure S2. Expression traditional fibroblast markers not restricted to fibroblasts or mesenchymal cells. A. Expression of traditional fibroblast markers in Gu dataset[56] and Dobnikar dataset[57], **B.** Expression of traditional fibroblast markers in spleen and bone marrow from Tabula Muris[58]. Annotation of cell types is according to the original papers.[56-58] **C-D.** Flow cytometry gating strategy and quantification of Ly6a/Sca-1 positivity in all vascular wall cell types, originating from thoracic aorta adventitia (N=4 groups, 7 young C57Bl6/J mice per group, total 28 mice). All results show mean ± SEM.

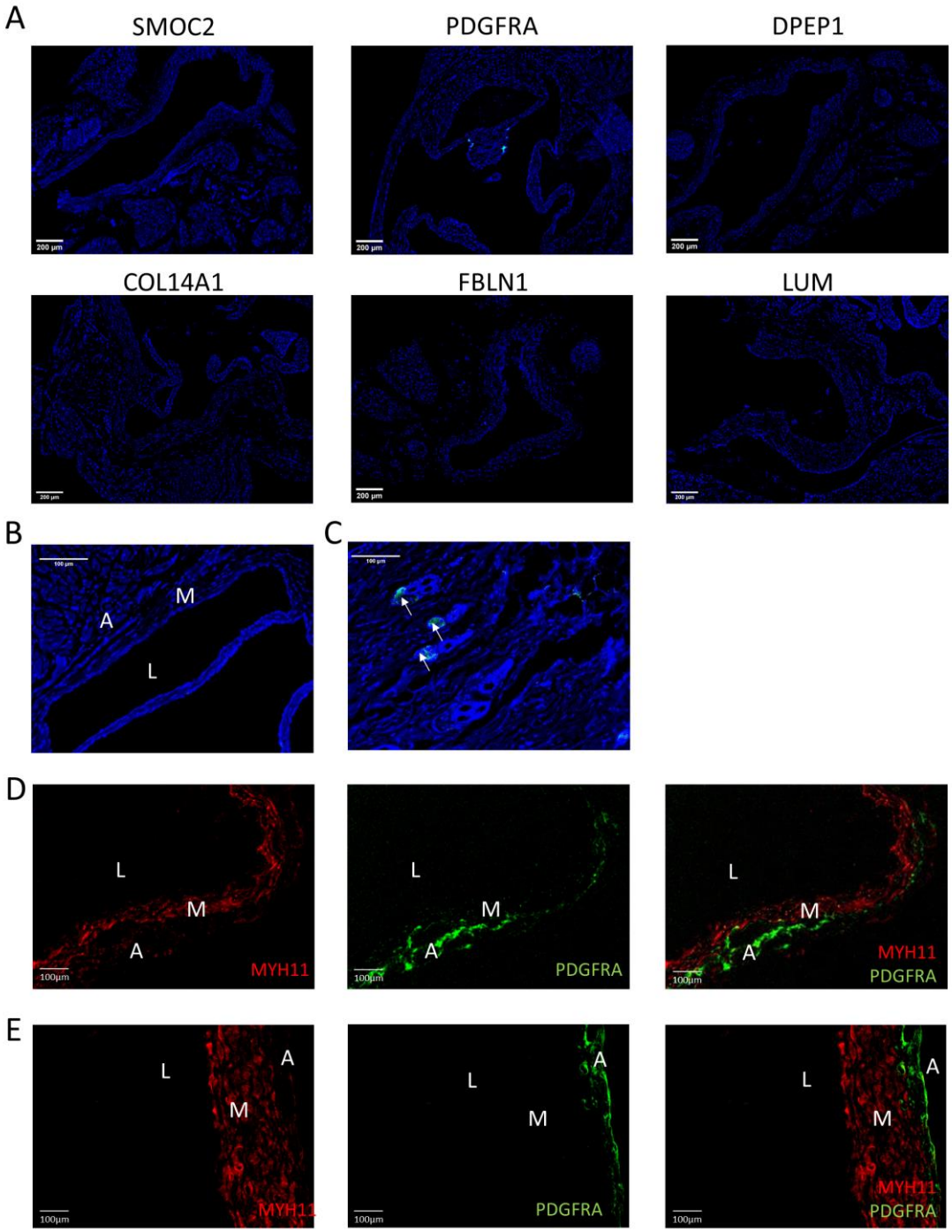

Supplemental Figure S3. Negative controls, immunohistochemical analysis of CCL11 in healthy C57BL/6J aortic roots, PDGFRA in Myh11-reporter mice and MYH11 in Pdgfra-reporter mice. A. Negative controls for immunohistochemical stainings of fibroblast signature markers, **B.** Murine aortic root immunohistochemically stained for Ccl11. Adventitia indicated by A, Media by M and Lumen by L., **C.** Positive control, murine dermis, with Ccl11 expression in green. **D.** PDGFRA expression in myosin heavy chain 11 (MYH11) reporter brachiocephalic artery. **E.** MYH11 expression in aortic root of Pdgfrα-TdTomato reporter. Myh11 in red, Pdgfrα in green, co-colaozaition (yellow) is absent. A indicates adventitia, M indicates media, and L indicates lumen.

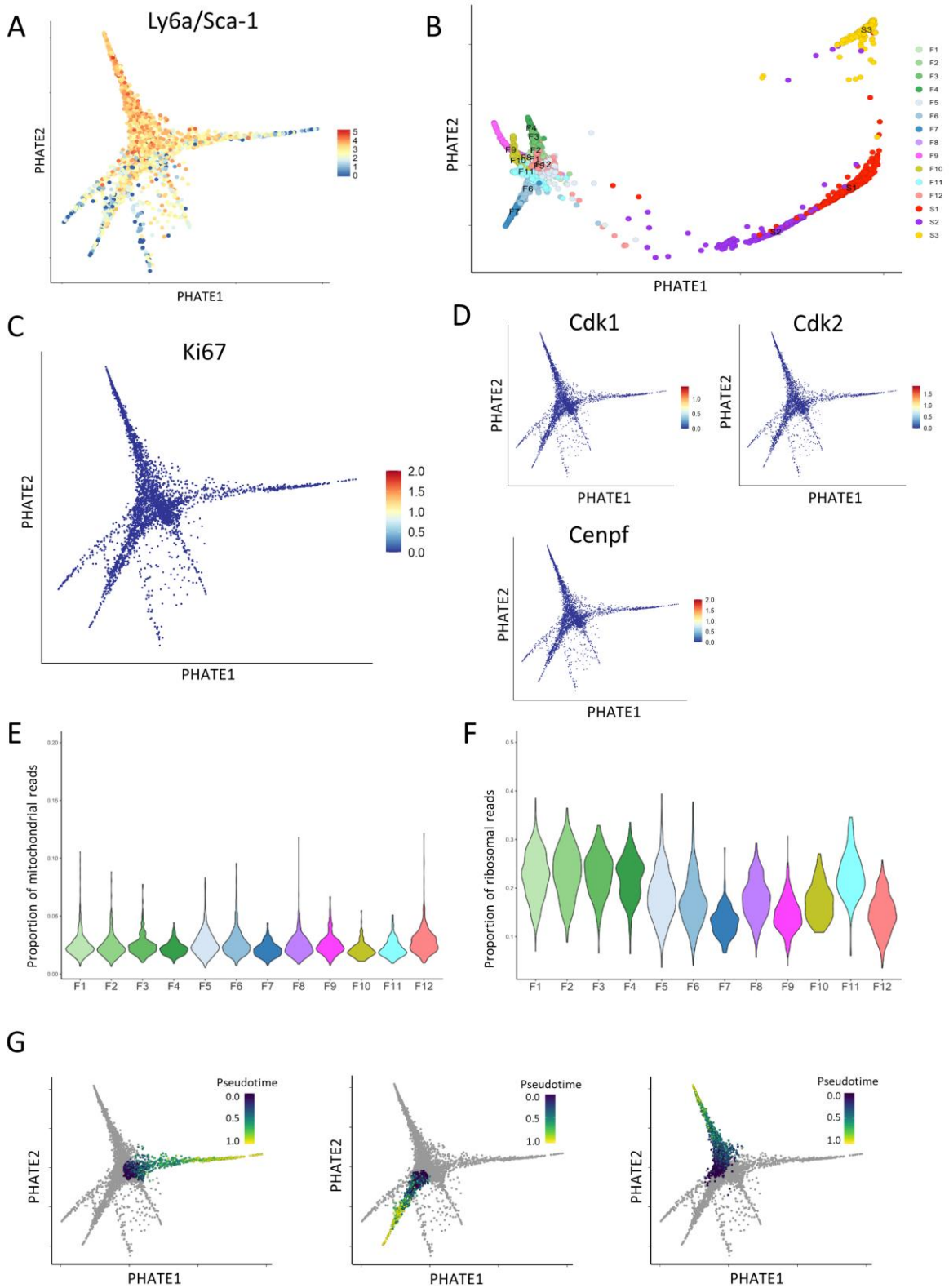

Supplemental figure S4. Expression of proliferation markers, mitochondrial genes or ribosomal genes absent in fibroblasts. A. *Ly6a/Sca-1* expression projected on PHATE plot of Figure 3A, **B.** PHATE dimensionality reduction on total dataset including fibroblasts and SMCs, **C.** *Ki67* expression projected on PHATE plot of Figure 3B, **D.** Expression of proliferation markers *Cdk1*, *Cdk2* and *Cenpf* projected on PHATE plot of Figure 3B, **E.** Proportion of mitochondrial genes among the twelve fibroblast clusters, **F.** Proportion of ribosomal genes among the twelve fibroblast clusters, **G.** Monocle pseudotime projection on each PHATE plot from figure 3B.

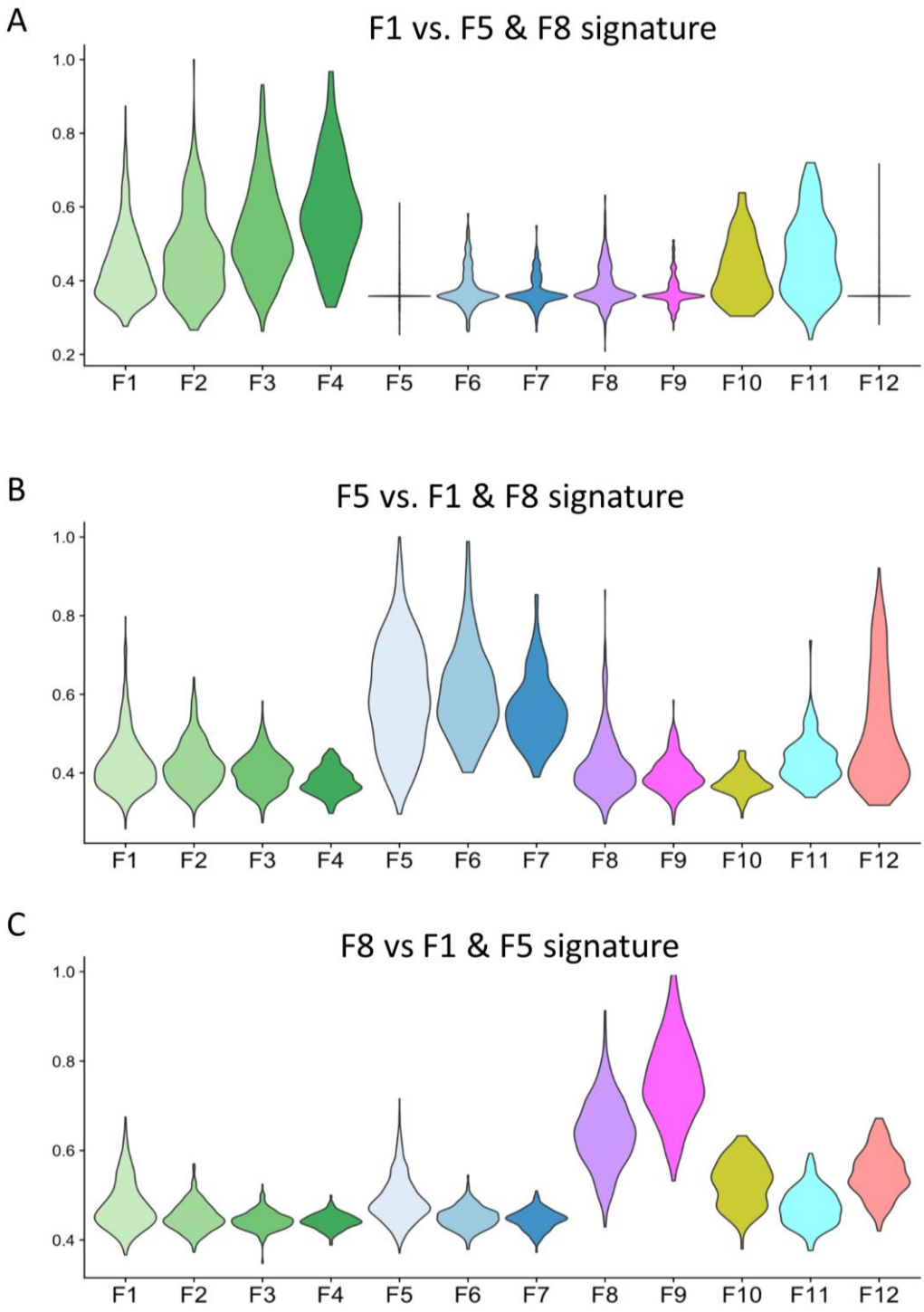

Supplemental figure S5. Gene signatures for the different core clusters per differentiation trajectory. A. Differential expression of signature for F1 vs F5+F8 in clusters F2, F3, F4 , and to a lesser extent F10 and F11, suggest these originate from F1, **B.** Differential expression of F5 vs F1+F8 signature in clusters F6, F7 and F12, **C.** Differential expression of F8 vs F5+F1 signature in population F9

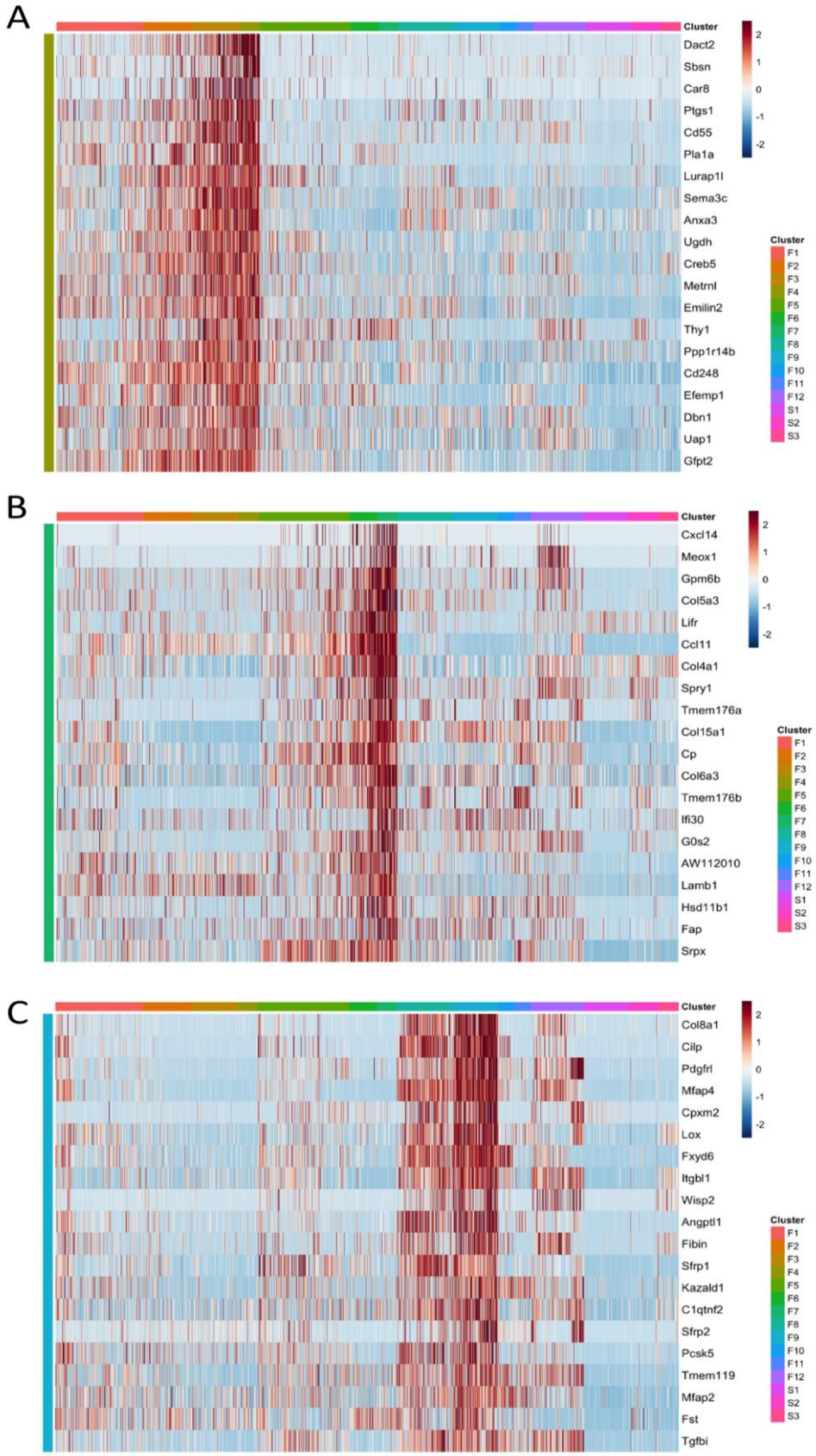

Supplemental Figure 6. Heatmaps depicting gene expression of trajectory specific markers. Heatmap for differentially expressed genes of trajectory 1 in **A**, trajectory 2 in **B** and trajectory 3 in **C**. Criteria included expression of genes in >70% of cells in end-cluster of each trajectory and <35% of remaining cells.

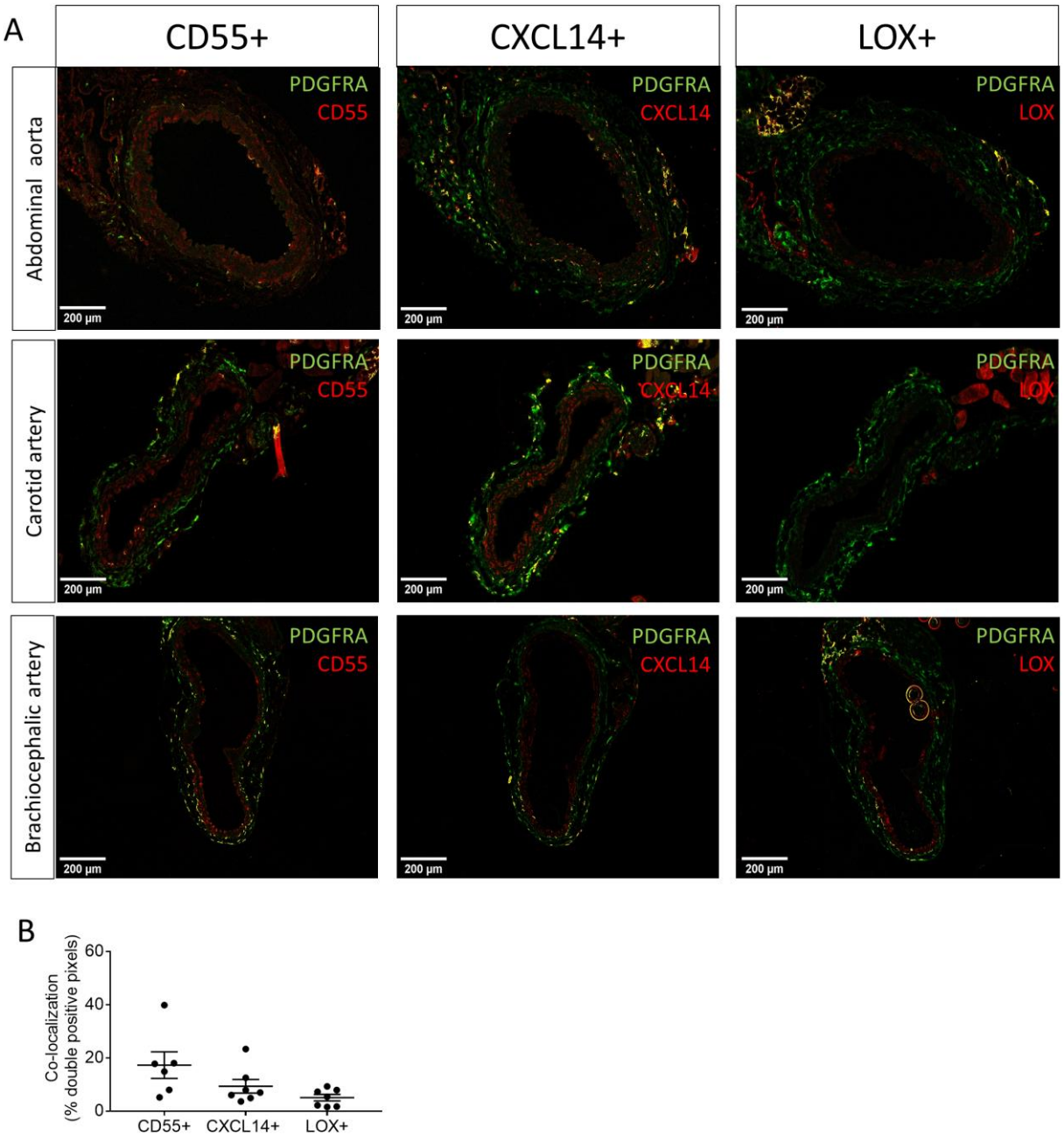

Supplemental Figure 7. Markers representing differentiated clusters presence in multiple vascular beds A. Immunohistochemical analysis of markers representing differentiated clusters for each trajectory in abdominal aorta, carotid artery and brachiocephalic artery (BCA), **B.** Quantification of co-localization of trajectory markers CD55, CXCL14 and LOX with PDGFRA in adventitia of healthy C57BL/6J brachiocephalic arteries. All results show mean ± SEM.

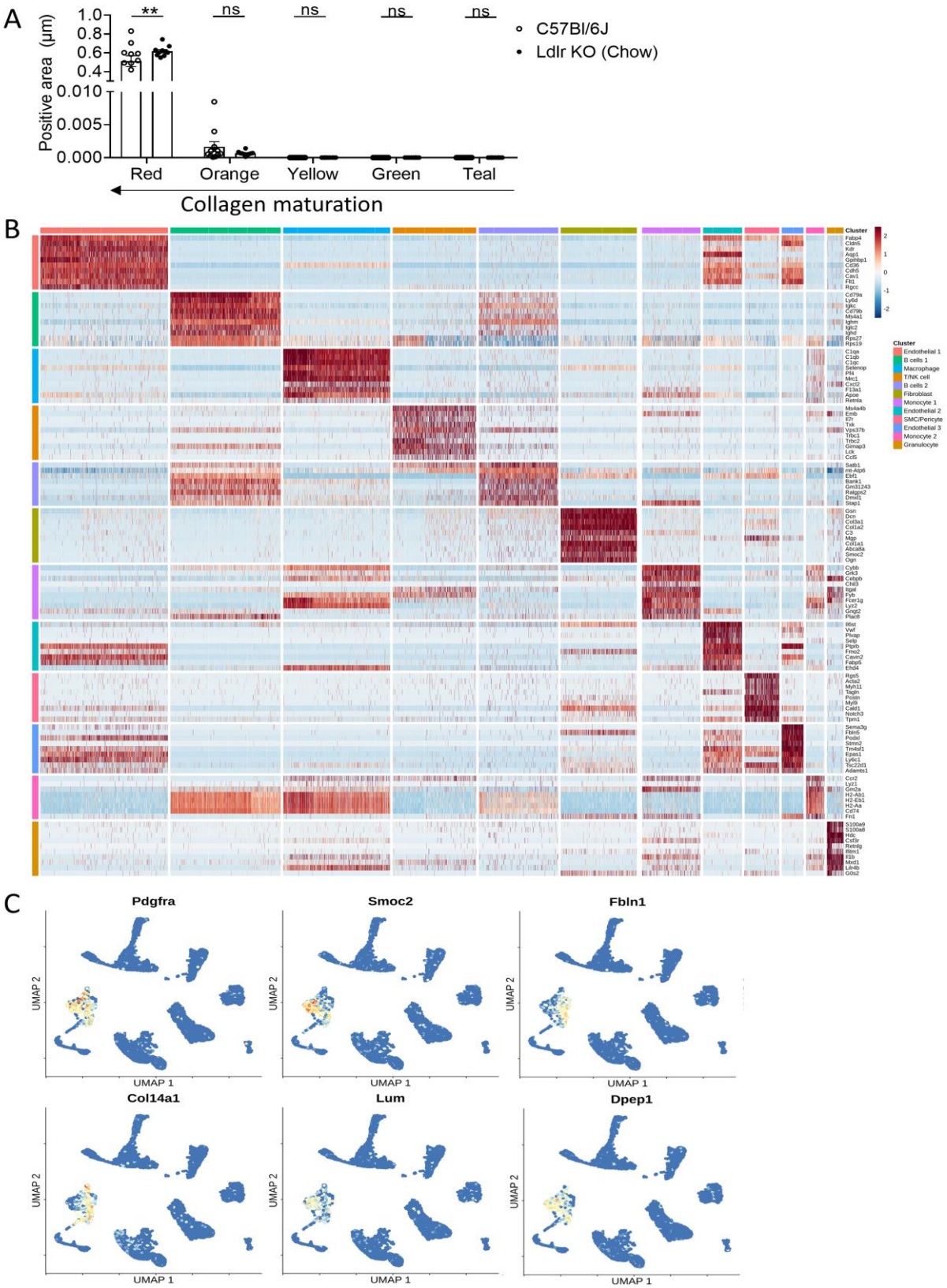

Supplemental Figure S8. Single cell sequencing of adventitia *Ldlr* KO mice A. Sirius red staining in adventitia of healthy C57BL/6J and Ldlr KO BCA. Red represents mature collagen, while teal presents the least mature collagen. **B.** Heatmap for cell annotation of single cell sequencing data, originating from *Ldlr* KO mice on chow and high cholesterol diet for 16 weeks, **B.** Annotation of fibroblasts in *Ldlr* KO single cell sequencing dataset making use of fibroblast-specific markers identified in Figure 2A. Visualization in UMAP. Statistical analyses were performed using two-way ANOVA with Bonferroni post-hoc test (A). All results show mean ± SEM **p<0.015

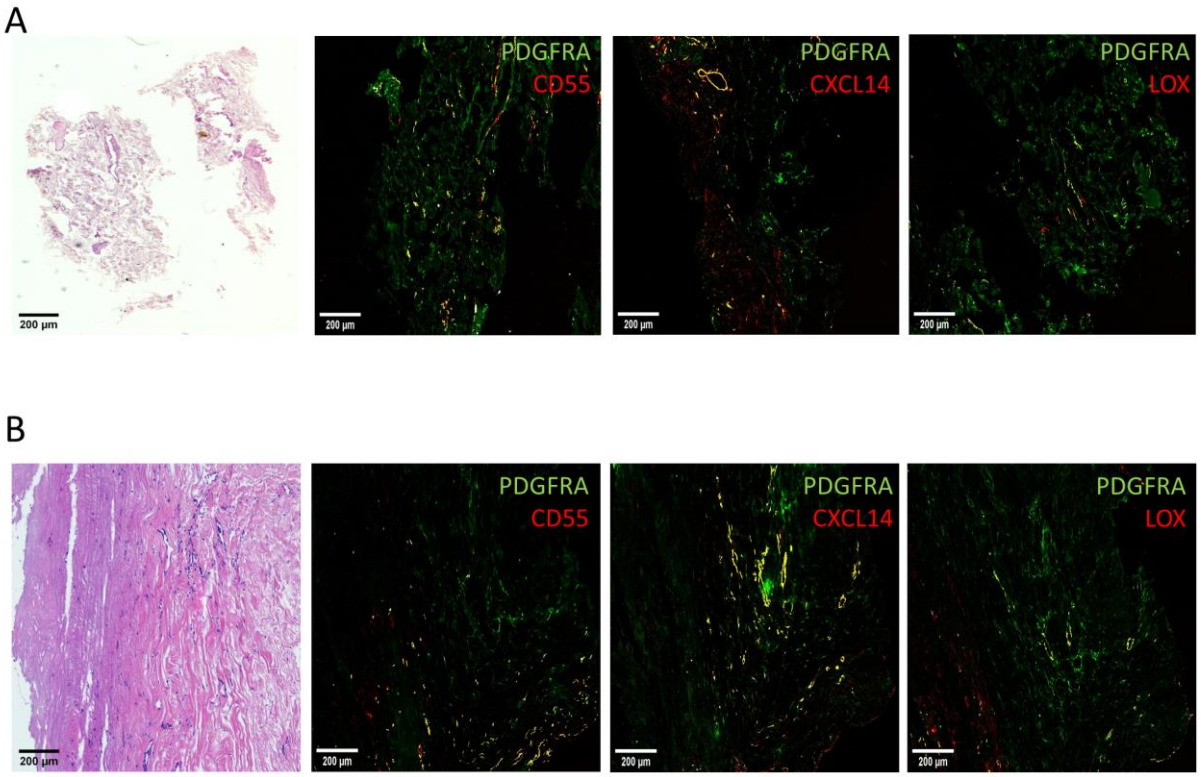

Supplemental Figure 9. Fibroblast trajectories in human specimens.
A. Immunohistochemical stainings of CD55+fibroblasts, CXCL14+fibroblasts, and LOX+ fibroblasts representing trajectory 1-3 respectively in specimens from carotid anastomosis during aortic bypass surgeries, **B.** Trajectory presence in human carotid adventitia, obtained from the opposite side of the culprit plaques during carotid endarterectomy, with corresponding H&E. Overlap between PDGFRA and trajectory markers is shown in yellow.

Legend Supplemental Video S1
Dissection of adventitia of the thoracic aorta (ranging from the aortic root until the diaphragm), which was carefully microscopically dissociated from the underlaying medial layer.

Supplemental Methods

Flow cytometry and cell sorting

Adventitia of the thoracic aorta (ranging from the aortic root until the diaphragm (Supplemental Video S1)) was carefully microscopically dissociated from the underlaying medial layer and collected in ice-cold PBS. Adventitial tissue of C57BL/6J or *Ldlr* KO mice was enzymatically digested for 15 minutes at 37°C using collagenase B (0.00284g/ml, Sigma 110088807001), pronase (0.01g/ml, Sigma 10165921001) and DNAse (0.1mg/ml, Roche 11284932001). This enzymatic cocktail ensures optimal isolation of mesenchymal cells[59]. Tissue was filtered through a 70µM strainer and subjected to red blood cell lysis (8.4g NH_4CL + 0.84g $NaHCO_3$ in 1 liter H_2O, pH 7.2-7.4). Living, DAPI-negative, mesenchymal cells were sorted as CD45 negative (BioLegend, 103114), and ICAM2 negative cells (BioLegend, 400526) on FACS Aria III for scRNA-seq in case of 8 week old C57BL/6J mice or living, DAPI-negative, cells for Ldlr KO mice.

Cells isolated from adventitia originating from either young C57BL/6J mice (8 weeks, male), aged C57BL/6J mice (72 weeks, male), *Ldlr* KO mice on chow or high cholesterol diet for 16 weeks were used for protein validation using flow cytometry (FACS canto II). After FC receptor blocking (15246827, Thermofisher) were stained with the following antibodies: CD45 (Biolegend, 103154), Cdh5/VE-cadherin (Invitrogen, 53-1441-82 or eBioscience 46-1441-82), Transgelin (Novus biologicals, NBP2-47689PCP or NBP2-47689AF488), Platelet derived growth factor alpha (PDGFRA) (BD Pharmingen, 562774), Sca-1/Ly6a (eBioscience 61-5981-82), CD55 (Biolegend, 131804), CXCL14 (Abcam, ab264467) and Lysyl oxidase (LOX) (Novus biologicals, NB-100-2527AF647), live/dead fixable cell stain (Invitrogen, L34957). In case of CXCL14, the antibody was labelled using a PE/Cy7 conjugation kit (Abcam, ab102903). For intracellular stainings (Transgelin, CXCL14 and LOX), fix & perm cell permeabilization kit was used (Invitrogen, GAS004). Data analysis was performed with BD FACS Diva software.

Single-cell sequencing

After cell count number and viability check with trypan blue (>85%), a total of ~16.000 adventitial CD45-/ICAM2- cells from healthy 8 weeks old, male C57BL/6J mice were loaded on a chromium single-cell controller using V2 reagent kit (10X Genomics). In case of *Ldlr* KO, a total of ~15.000 cells were loaded using V2 reagent kit (10X Genomics). Samples were loaded approximately 4 hours after tissue isolation. Libraries of cDNA were synthesized as suggested by 10X genomics and used to create sequencing libraries. In short, in reaction vesicles (gel beads in emulsion, GEMs), cells were lysed and barcoded oligonucleotides reverse transcribed before clean-up and cDNA amplification. The Chromium Single-Cell 3' Library Kit was then used to generate indexed sequencing libraries. Sequencing was performed on Illumina HiSeq4000. In case of C57BL/6J, 5701 cells were yielded with ~87,000 reads per cell and for *Ldlr* KO, 4800 cells were yielded after chow diet and ~8000 cells after HCD, with 63,000 and 47,390 reads per cell respectively (Supplemental Tables 1-2).

Immunohistochemical stainings

Murine tissue was fixed in 1% paraformaldehyde overnight, paraffin-embedded, and serially sectioned (4µm). For stainings, only sections that had mature media (determined by elastin fiber presence) were used. Tissue was deparaffinized using Xylene and rehydrated using an alcohol gradient (100-50% in dH_2O). Antigen retrieval was performed using low pH EnVision Dako target retrieval solution (Dako K800521-2), followed by blocking in 10% normal swine serum (Dako, X0901) in tris buffered saline (TBS). Immunohistochemical detection of the following antigens was performed: SMOC2 (Biorbyt, orb525072), COL14A1 (Novus biologicals, NBP2-15940), mouse PDGFRA (R&D, BAF1062), human PDGFRA (R&D, AF-307-NA), FBLN1 (Human Protein Atlas, HPA001613), LUMICAN (Abcam, ab168348), CCL11 (R&D, AF-420-NA), DPEP1 (Abcam, ab121308), MAC3 (Becton Dickinson), CD55 (ThermoFisher, PA5-78991), mouse CXCL14 (Abcam, ab13741), human CXCL14 (Proteintech, 10468-1-AP), LOX (Novus Biologicals, NB100-2527), Collagen type I (Abcam, ab21286), Vimentin (Abcam ab92547), CD90 (Biolegend 105307), and total collagen

(Picosirius red, Polyscience 09400). Rabbit host primary antibodies were detected with a swine anti-rabbit secondary antibody (Dako, E0431), goat host primary antibodies were detected with a rabbit anti-goat secondary antibody (Dako, E046601-2), followed by signal amplification using Vectastain-ABC (Vector, AK-5000). Visualization was performed with 3,3'-diaminobenzidine (DAB, Agilent K346811-2) for single stains, while double stains were visualized with Vector Red/Blue (Vector, SK5100/5300). Pseudo-fluorescent images were created and adventitial co-localization quantified using the Nuance Multispectral Imaging System or Fiji. Quantification of adventitial area (Defined as the area where medial elastin fibers end and the width is roughly similar to the width of the media), collagen 1 content (% adventitial area), and MAC3 (n/mm2 adventitia) was done on images scanned with the Histotech P1000 scanner and analyzed with Qupath (v0.2.0-m8), while Sirius red was quantified on 20X images using Leica Qwin software. Representative images were selected based on the mean value of the corresponding analysis. Please see the Major Resources Table in the Supplemental Materials for additional details on antibodies.

Human sample analysis

Human tissue collection was part of the Maastricht Pathology Tissue Collection (MPTC) and further storage and use of the tissue was in line with the Dutch Code for Proper Secondary use of Human Tissue and the local Medical Ethical Committee (protocol number 16-4-181). This code (https://www.federa.org/codes-conduct) entails an opt-out arrangement and hence tissues were not used in case of objection. The applicability of this code for this study was approved by the Maastricht University hospital (MUMC) local Medical Ethical Committees. Human studies conducted by Li et al.[60] and Wirka et al.[61] are approved by Institutional Review Board at Baylor College of Medicine and Stanford University Institutional Review Board, respectively, and follow the guidelines of the Declaration of Helsinki. Written informed consent was provided by all participants or the organ donors' legal representatives before enrollment. Formalin-fixed, paraffin-embedded (FFPE) carotid arteries were collected at autopsy (n=10), or from patients undergoing carotid endarterectomy (CEA) (n=63 plaques, 43 patients), opposite the plaque (n=10), or at carotid anastomosis during aorta bypass surgery (n=10). 5mm-segments were alternated with frozen segments for histology and RNA isolation in case of CEA. A total of 43 plaque segments were collected from 23 symptomatic patients undergoing CEA in the Maastricht Human Plaque Study (MaasHPS) were used for further microarray analysis. Library preparation, RNA extraction, data processing, normalization and additional information concerning plaque traits have been described in great detail elsewhere[62, 63].

Quantification and Statistical analysis

Single-cell sequencing analysis C57BL/6J mice

The 10X Cell Ranger pipeline (v2.1.1) was used to perform alignment of raw sequencing reads to the mouse reference genome (mm10), filtering, barcode, and unique molecular identifiers (UMI) counting. Generated filtered expression matrices were subsequently used for additional quality control and subsequent analysis using the Seurat (v2.3) R package[64]. Initial quality control was performed by removing low quality cells found to express less than 1500 genes, those with a UMI count greater 15,000, or those with more than 15% of reads aligning to mitochondrial genes (mito%, 654 cells removed in total). Global data normalization was then performed using the Normalize Data method[64], which normalizes gene expression in individual cells based on the total gene expression, followed by multiplying by a factor of 10,000, and transforming the data by $\log_e$. Data was then scaled using the ScaleData method[64] and dimensionality reduction was performed using principal component analysis (PCA). PCA was carried out using the most variable genes in the dataset, identified by the FindVariableGenes method[64] selecting genes with a log variance to mean ratio (VMR) greater than 0.1. The appropriate number of principal components to be used for graph-based clustering and t-distributed stochastic neighbour embedding (tSNE) construction was determined by choosing the principal component (PC) after which the standard deviation of subsequent PCs remained approximately constant. Cluster identification was performed using the FindClusters method[64] using PCA as the chosen method of dimension reduction. Identified clusters were then

visualized on a tSNE plot constructed using the appropriate number of PCs. Clusters found to have a low proportion of cells expressing *Pdgfrb* or containing cells positive epithelial markers (*Krt19*, *Lgals7*, and *Cd82*) were removed from the dataset prior to re-clustering as described above (639 cells in total). Identified clusters were categorized based on their marker gene expression as either being smooth muscle (672 cells positive for *Myh11, Acta2, Tagln, Cnn1*) or fibroblast-like (3736 cells positive for *Col1a1, Col1A2, Ly6a, Mmp2*). Differential gene expression analysis compared smooth muscle cells to fibroblasts cells using the FindAllMarkers command [64]. Only genes expressed in a minimum of 33% of cells in the given cell type, with a minimum $\log_e$ fold change (logFC) in expression of 0.25, and with a difference in the fraction of positive cells between groups of at least 33%. Significantly differentially expressed markers were identified by the Wilcoxon rank sum test as having a Bonferroni adjusted P value <0.05. The top 20 markers based on logFC from each cell type were used for heatmap construction. Cell type markers were similar with mito% <10% and <15%.

Following sub-setting of data to contain only fibroblast-like cells, PHATE dimension reduction[65] was performed using the most variable genes in the fibroblast dataset. Highly variable genes were selected with an average expression (quantified as normalized ln(UMI+1)) between 0.05 and 4 and with a log VMR between 0.075 and 10. Cluster identification within the fibroblast dataset was performed using the FindClusters method [64] with PHATE[65] used as the dimension reduction method. Identified clusters were then visualized on the PHATE plot using the DimPlot command [64]. Markers from each fibroblast cluster were identified using the FindAllMarkers method [64] selecting genes only expressed in at least 25% of cells within the given cluster and with a logFC in expression threshold of at least 0.2. Comparative scRNA-seq datasets were imported directly as filtered count matrices and processed in accordance with the methods from the accompanying publications[18,28,30,56].

Single-cell sequencing analysis *Ldlr* KO mice

Filtered count matrices were generated using the 10X CellRanger V3.0.2 pipeline using the standard GRCh38-3.0.0 genome reference downloaded from 10X genomics (10X Genomics, Pleasanton, USA). The R package scater was used to perform cell filtering quality control on individual datasets [66]. Cells with a UMI count exceeding 3 median absolute deviations (MADs) from the median UMI value were excluded from downstream analysis. Similarly, cells with a total gene count less than 200 genes or with a high proportion of reads originating from mitochondrial genes (>4MADs) were also excluded. Prior to combining the two datasets, data normalisaton was performed using the MultiBatchNormalisation method [67]. Mitochondrial and ribosomal genes were excluded from the 2000 highly variable genes identified using the FindVariableFeatures function and the 'vst' selection method in Seurat V3.2.3 [68]. Following scaling of data, principal component analysis was performed using the previously identified list of highly variable genes. Clustering of cells was performed using the standard 'FindNeighbours' and 'FindClusters' methods including the first 12 principal components [68]. Clustered data was then visualised in two dimensions using the Manifold Approximation and Projection (UMAP) method calculated using the 'RunUMAP' command [68]. Differential gene expression analysis was performed using the 'FindAllMarkers' method selecting markers expressed in at least 30% of cells in the corresponding cluster and with a minimum log fold change in expression of 0.3 compared to the remainder of the dataset. Count data from cells belonging to the identified fibroblast cluster was extracted to further explore fibroblast heterogeneity using the same processing steps described above. Contaminating schwann and mesothelial cells were excluded from further analysis of fibroblast heterogeneity. PHATE reduction analysis was performed as described below [69]. Published datasets were reanalysed per published methods[56, 57, 60, 61, 70, 71].

Cell signature scores

Cell signature scores were calculated as the scaled geometric mean of the expression of selected marker genes within each cell. All gene names within the dataset beginning with 'Mt' were included for generating the mitochondrial signature. All gene names beginning with 'Rpl' or 'Rps' within the dataset were included for calculating the ribosomal signature.

Pseudotime and RNA velocity analysis

Pseudotime cellular trajectories were calculated with the Monocle package (v2.10.1)[72]. Subsets of fibroblast cells were first produced based on the localization of clusters within the branches of the previously generated PHATE plot. The FindMarkers method[64] was then used to identify markers of clusters localizing at the beginning and end of each PHATE branch. Marker genes with the highest logFC in expression were subsequently used for dimensionality reduction of data to two dimensions using the reduceDimension method[72]. Pseudotime values were then calculated using the orderCells command applying default Monocle parameters[72]. Following scaling from 0 to 1, pseudotime values were subsequently mapped onto the corresponding cells on the previously generated PHATE plots. Directionality of cellular transitions were inferred by calculating the RNA velocity of individual cells using the velocyto R package[73]. Reads were identified as mapping to either intronic or exonic sequences using the DropEst pipeline [74] utilising the previously generated binary alignment files from the Cell Ranger pipeline. Velocyto was then used to calculate RNA velocity using KNN pooling with Kcells = 25 and gamma fit performed using the full range of cellular expression magnitudes. RNA velocity vectors were then superimposed onto the previously generated PHATE plot.

Functional analysis using gene ontology (GO) terminology

Functional enrichment analysis was performed using G:profiler[75]. A ranked list of the differentially expressed genes per end cluster was used as input. To increase the interpretative value, the size of the functional category range was set from 5 to 750. Electronic GO annotations were disabled and the size of query/term intersection was set to 3 to increase the reliability [76]. The top-10 Go biological process terms per cluster were selected and plotted on an excel bubble chart where the diameter of the node represents the -log10(p-Value).

Enrichment analysis using hypergeometric testing

The DEGs from the full trajectories (F1, F2, F3, F4, n = 216; F5, F6, F7, n = 235; F8, F9, n = 317) were intersected with 1) GWAS CAD-associated genes, and 2) human aorta fibroblast DEGs from the study of Li et al[60]. For this, a total of 329 CAD-associated genes were retrieved from the GWAS association file (v1.0, 2021-12-07; downloaded from the GWAS Catalog[77] website: https://www.ebi.ac.uk/gwas/) by searching the key word “coronary” in the term “disease/trait”. In addition, for each of the four human aorta fibroblast clusters reported by Li et al., we downloaded the top 20 DEGs from the original paper[60] and combined them as a comprehensive fibroblast gene set. Hypergeometric testing was used to evaluate the statistical significance of the overlap genes between trajectory genes and CAD or fibroblast genes. Mouse genes were converted to human genes by biomaRt R package (v2.50.1)[78].

Data availability

Data are deposited in a repository (GSE196395),and may be inspected on a web-based interface (Plaqview.com)[79]. Count matrices and code are available upon reasonable request.

Statistical analysis

For human samples, correlations between genes and clinical traits were calculated using Pearson’s Correlation Coefficient. Only pairwise complete observations were included if missing values were contained in traits. Student P-value was calculated based on the correlations and sample size. Normality of the data was assessed through D’Agostino-Pearson omnibus normality test and potential outliers were identified through the ROUT method. For mice flow cytometry analysis and Sirius red quantification, an ordinary two-way ANOVA was performed, followed by Tukey’s multiple comparisons test. For immunohistochemistry analyses, depending on number of groups unpaired T-test with Welch’s correction or one-way ANOVA was used, followed by Bonferroni’s multiple comparisons test. Statistical testing was done using Graphpad Prism 7.0.

Supplemental References

56. Gu W, Ni Z, Tan YQ, Deng J, Zhang SJ, Lv ZC, Wang XJ, Chen T, Zhang Z, Hu Y, Jing ZC, Xu Q. Adventitial Cell Atlas of wt (Wild Type) and ApoE (Apolipoprotein E)-Deficient Mice Defined by Single-Cell RNA Sequencing. *Arterioscler Thromb Vasc Biol* 2019;**39**:1055-1071.
57. Dobnikar L, Taylor AL, Chappell J, Oldach P, Harman JL, Oerton E, Dzierzak E, Bennett MR, Spivakov M, Jorgensen HF. Disease-relevant transcriptional signatures identified in individual smooth muscle cells from healthy mouse vessels. *Nat Commun* 2018;**9**:4567.
58. Tabula Muris C. Single-cell transcriptomics of 20 mouse organs creates a Tabula Muris. *Nature* 2018;**562**:367-372.
59. Ramachandran P, Dobie R, Wilson-Kanamori JR, Dora EF, Henderson BEP, Luu NT, Portman JR, Matchett KP, Brice M, Marwick JA, Taylor RS, Efremova M, Vento-Tormo R, Carragher NO, Kendall TJ, Fallowfield JA, Harrison EM, Mole DJ, Wigmore SJ, Newsome PN, Weston CJ, Iredale JP, Tacke F, Pollard JW, Ponting CP, Marioni JC, Teichmann SA, Henderson NC. Resolving the fibrotic niche of human liver cirrhosis at single-cell level. *Nature* 2019;**575**:512-518.
60. Li Y, Ren P, Dawson A, Vasquez HG, Ageedi W, Zhang C, Luo W, Chen R, Li Y, Kim S, Lu HS, Cassis LA, Coselli JS, Daugherty A, Shen YH, LeMaire SA. Single-Cell Transcriptome Analysis Reveals Dynamic Cell Populations and Differential Gene Expression Patterns in Control and Aneurysmal Human Aortic Tissue. *Circulation* 2020;**142**:1374-1388.
61. Wirka RC, Wagh D, Paik DT, Pjanic M, Nguyen T, Miller CL, Kundu R, Nagao M, Coller J, Koyano TK, Fong R, Woo YJ, Liu B, Montgomery SB, Wu JC, Zhu K, Chang R, Alamprese M, Tallquist MD, Kim JB, Quertermous T. Atheroprotective roles of smooth muscle cell phenotypic modulation and the TCF21 disease gene as revealed by single-cell analysis. *Nat Med* 2019;**25**:1280-1289.
62. Jin H, Goossens P, Juhasz P, Eijgelaar W, Manca M, Karel JMH, Smirnov E, Sikkink C, Mees BME, Waring O, van Kuijk K, Fazzi GE, Gijbels MJJ, Kutmon M, Evelo CTA, Hedin U, Daemen M, Sluimer JC, Matic L, Biessen EAL. Integrative multiomics analysis of human atherosclerosis reveals a serum response factor-driven network associated with intraplaque hemorrhage. *Clin Transl Med* 2021;**11**:e458.
63. Jin H, Mees BME, Biessen EAL, Sluimer JC. Transcriptional Sex Dimorphism in Human Atherosclerosis Relates to Plaque Type. *Circ Res* 2021;**129**:1175-1177.
64. Butler A, Hoffman P, Smibert P, Papalexi E, Satija R. Integrating single-cell transcriptomic data across different conditions, technologies, and species. Nat Biotechnol. United States, 2018:411-420.
65. Kevin R. Moon DvD, Zheng Wang, Scott Gigante, Daniel B. Burkhardt, William S. Chen, Kristina Yim, Antonia van den Elzen, Matthew J. Hirn, Ronald R. Coifman, Natalia B. Ivanova, Guy Wolf, Smita Krishnaswamy. PHATE: A Dimensionality Reduction Method for Visualizing Trajectory Structures in High-Dimensional Biological Data. *bioRxiv* 2017.
66. McCarthy DJ, Campbell KR, Lun AT, Wills QF. Scater: pre-processing, quality control, normalization and visualization of single-cell RNA-seq data in R. *Bioinformatics* 2017;**33**:1179-1186.
67. Haghverdi L, Lun ATL, Morgan MD, Marioni JC. Batch effects in single-cell RNA-sequencing data are corrected by matching mutual nearest neighbors. *Nat Biotechnol* 2018;**36**:421-427.
68. Stuart T, Butler A, Hoffman P, Hafemeister C, Papalexi E, Mauck WM, 3rd, Hao Y, Stoeckius M, Smibert P, Satija R. Comprehensive Integration of Single-Cell Data. *Cell* 2019;**177**:1888-1902 e1821.
69. Moon KR, van Dijk D, Wang Z, Gigante S, Burkhardt DB, Chen WS, Yim K, Elzen AVD, Hirn MJ, Coifman RR, Ivanova NB, Wolf G, Krishnaswamy S. Visualizing structure and transitions in high-dimensional biological data. *Nat Biotechnol* 2019;**37**:1482-1492.
70. Cochain C, Vafadarnejad E, Arampatzi P, Pelisek J, Winkels H, Ley K, Wolf D, Saliba AE, Zernecke A. Single-Cell RNA-Seq Reveals the Transcriptional Landscape and

Heterogeneity of Aortic Macrophages in Murine Atherosclerosis. *Circ Res* 2018;**122**:1661-1674.
71. Dawson A, Li Y, Li Y, Ren P, Vasquez HG, Zhang C, Rebello KR, Ageedi W, Azares AR, Mattar AB, Sheppard MB, Lu HS, Coselli JS, Cassis LA, Daugherty A, Shen YH, LeMaire SA. Single-Cell Analysis of Aneurysmal Aortic Tissue in Patients with Marfan Syndrome Reveals Dysfunctional TGF-beta Signaling. *Genes (Basel)* 2021;**13**.
72. Trapnell C, Cacchiarelli D, Grimsby J, Pokharel P, Li S, Morse M, Lennon NJ, Livak KJ, Mikkelsen TS, Rinn JL. The dynamics and regulators of cell fate decisions are revealed by pseudotemporal ordering of single cells. *Nat Biotechnol* 2014;**32**:381-386.
73. La Manno G, Soldatov R, Zeisel A, Braun E, Hochgerner H, Petukhov V, Lidschreiber K, Kastriti ME, Lonnerberg P, Furlan A, Fan J, Borm LE, Liu Z, van Bruggen D, Guo J, He X, Barker R, Sundstrom E, Castelo-Branco G, Cramer P, Adameyko I, Linnarsson S, Kharchenko PV. RNA velocity of single cells. *Nature* 2018;**560**:494-498.
74. Petukhov V, Guo J, Baryawno N, Severe N, Scadden DT, Samsonova MG, Kharchenko PV. dropEst: pipeline for accurate estimation of molecular counts in droplet-based single-cell RNA-seq experiments. *Genome Biol* 2018;**19**:78.
75. Raudvere U, Kolberg L, Kuzmin I, Arak T, Adler P, Peterson H, Vilo J. g:Profiler: a web server for functional enrichment analysis and conversions of gene lists (2019 update). *Nucleic Acids Res* 2019;**47**:W191-W198.
76. Reimand J, Isserlin R, Voisin V, Kucera M, Tannus-Lopes C, Rostamianfar A, Wadi L, Meyer M, Wong J, Xu C, Merico D, Bader GD. Pathway enrichment analysis and visualization of omics data using g:Profiler, GSEA, Cytoscape and EnrichmentMap. *Nat Protoc* 2019;**14**:482-517.
77. Buniello A, MacArthur JAL, Cerezo M, Harris LW, Hayhurst J, Malangone C, McMahon A, Morales J, Mountjoy E, Sollis E, Suveges D, Vrousgou O, Whetzel PL, Amode R, Guillen JA, Riat HS, Trevanion SJ, Hall P, Junkins H, Flicek P, Burdett T, Hindorff LA, Cunningham F, Parkinson H. The NHGRI-EBI GWAS Catalog of published genome-wide association studies, targeted arrays and summary statistics 2019. *Nucleic Acids Res* 2019;**47**:D1005-D1012.
78. Durinck S, Spellman PT, Birney E, Huber W. Mapping identifiers for the integration of genomic datasets with the R/Bioconductor package biomaRt. *Nat Protoc* 2009;**4**:1184-1191.
79. Ma WF, Hodonsky CJ, Turner AW, Wong D, Song Y, Mosquera JV, Ligay AV, Slenders L, Gancayco C, Pan H, Barrientos NB, Mai D, Alencar GF, Owsiany K, Owens GK, Reilly MP, Li M, Pasterkamp G, Mokry M, van der Laan SW, Khomtchouk BB, Miller CL. Enhanced single-cell RNA-seq workflow reveals coronary artery disease cellular cross-talk and candidate drug targets. *Atherosclerosis* 2022;**340**:12-22.